IEEE Access
Multidisciplinary | Rapid Review | Open Access Journal

Received March 3, 2022, accepted March 17, 2022, date of publication March 28, 2022, date of current version April 5, 2022.

Digital Object Identifier 10.1109/ACCESS.2022.3162751

Generalized Quadrature Index Modulation With Multi-Index and Dimension-Extended Constellation

ZHENYU TANG[1], FUCHUN HUANG[2], ZHILI ZHOU[3], ZHIJUN LIU[1], AND QILIN BI[1]
[1]School of Ship and Marine Engineering, Guangzhou Maritime University, Guangzhou 510725, China
[2]Guangzhou College of Commerce, Guangzhou 511363, China
[3]School of Electrical and Electronic Engineering, Wenzhou University, Wenzhou 325035, China

Corresponding author: Zhili Zhou (zhouzhili@wzu.edu.cn)

This work was supported in part by the Major Science and Technology Projects in Guangdong Province under Grant 2017B010118004, and in part by the Guangzhou Science and Technology Planning Project under Grant 201904010205.

ABSTRACT In this paper, in pursuit of enhancing the spectral efficiency and reliability of transmission in multiple-input multiple-output (MIMO) communication system, a new design method, named as the generalization of quadrature index modulation (GQIM), is proposed. In GQIM system, the key and vector indications are exploited by the design of the transmitted spatial vector (TSV). Also, the transmit diversity gain by transmitting two versions produced by a three dimension (3D) symbol is achieved. More specifically, in our proposed GQIM system, an extended dimension signal constellation, so called extended 3D constellation (E3DC), is designed for the employment in the GQIM framework. Then, for achieving the transmit diversity gain, combing with the antenna indexes, the X-axis, Y-axis, Z-axis components of two versions of the E3D symbol are constructed into four spatial vectors that are considered as candidates of the real/imaginary part of a complex TSV. Furthermore, two possible TSVs are obtained by using two adders and two key controllers with two states of 1 and j. With the aid of the vector indication, one out of two possible TSVs is selected for transmission. Finally, the spectral efficiency and squared MED, the spatial index bits and computational complexity, the upper bound on the average bit error probability are analyzed. The analytical and simulation results demonstrate the correctness of GQIM and show that GQIM achieves a higher data rate and the reliability of transmission in comparison to the existing classic systems.

INDEX TERMS Generalization of quadrature index modulation (GQIM), the key and vector indications, transmit diversity gain, extended dimension signal constellation, extended 3D constellation (E3DC), a complex TSV.

I. LIST OF ACRONYMS

The acronyms used in this paper are listed as follows:

AI	Antenna Index.
BER	Bit Error Rate.
SM	Spatial Modulation.
SSK	Space Shift Keying.
PSK	Phase Shift Keying.
CCI	Co-channel Interferences.
CP	Signal Constellation Point.
TSV	Transmitted Spatial Vector.
GSM	Generalized Spatial Modulation.
QSM	Quadrature Spatial Modulation.
DSM	Double Spatial Modulation.
ESM	Enhanced Spatial Modulation.
MED	Minimum Euclidean Distance.
E3DC	Extended 3D Constellation.
QAM	Quadrature Amplitude Modulation.
MIMO	Multiple Input Multiple Output.
MIMO-IM	MIMO with Index Modulation.
V-BLAST	Vertical Bell Labs Layered Space-Time.
GQIM	Generalized Quadrature Index Modulation.
SM-SC	Spatial Modulation with Spatial Constellation.
QIM-TDC	Quadrature Index Modulation with Three Dimension Constellation.
GSM-MIM	Generalized Spatial Modulation with Multi-Index Modulation.

The associate editor coordinating the review of this manuscript and approving it for publication was Zhen Gao.

This work is licensed under a Creative Commons Attribution 4.0 License. For more information, see https://creativecommons.org/licenses/by/4.0/

II. LIST OF SYMBOLS

The symbols used in this paper are listed as follows:

N_{t}	Number of transmit antennas.
N_{r}	Number of receive antennas.
$\mathbf{S}$	Transmitted spatial vector.
$\bar{\mathbf{S}}$	Normalized TSV symbol.
I_{B}	Transmission rate.
S_{3D}	E3D constellation symbol.
I_s	The number of bits that E3D symbols carried.
M	The modulation order of E3D constellation.
N	The modulation order of APM constellation.
I_{C}	The number of bits that APM symbols carried.
I_ε	The sign indication bit.
I_{SI}	The total number of spatial index bits.
I_{k}	One bit that the real/imaginary key carried.
$I_{\mathbf{V}}$	One bit that the TSV key carried.
I_{AI}	The total number of bits for the AI vector sets.
$\Omega_{\mathrm{A}}/\Omega_{\bar{\mathrm{A}}}$	The AI vector set including $\frac{N_{\mathrm{t}}}{2}$ vectors.
$\Omega_{\mathrm{B}}/\Omega_{\bar{\mathrm{B}}}$	The AI vector set including $\frac{N_{\mathrm{t}}}{4}$ vectors.
$\Omega_{\mathrm{C}}/\Omega_{\bar{\mathrm{C}}}$	The AI vector set including $\frac{N_{\mathrm{t}}}{4}$ vectors.
$I_{\mathrm{A}}/I_{\bar{\mathrm{A}}}$	The number of bits that the AI set $\Omega_{\mathrm{A}}/\Omega_{\bar{\mathrm{A}}}$ carried.
$I_{\mathrm{B}}/I_{\bar{\mathrm{B}}}$	The number of bits that the AI set $\Omega_{\mathrm{B}}/\Omega_{\bar{\mathrm{B}}}$ carried.
$I_{\mathrm{C}}/I_{\bar{\mathrm{C}}}$	The number of bits that the AI set $\Omega_{\mathrm{C}}/\Omega_{\bar{\mathrm{C}}}$ carried.
$\mathbf{e}_\alpha/\mathbf{e}_{\bar{\alpha}}$	The $\alpha/\bar{\alpha}$-th column of the identity matrix $\mathbf{I}_{\frac{N_{\mathrm{t}}}{2}}$.
$\mathbf{I}_{\frac{N_{\mathrm{t}}}{2}}$	The identity matrix with $(\frac{N_{\mathrm{t}}}{2} \times \frac{N_{\mathrm{t}}}{2})$ dimensions.
$\mathbf{B}_\beta/\bar{\mathbf{B}}_{\bar{\beta}}$	The $\beta/\bar{\beta}$-th column vector of the AI set $\Omega_{\mathrm{B}}/\Omega_{\bar{\mathrm{B}}}$.
$\mathbf{C}_\gamma/\bar{\mathbf{C}}_{\bar{\gamma}}$	The $\gamma/\bar{\gamma}$-th column vector of the AI set $\Omega_{\mathrm{C}}/\Omega_{\bar{\mathrm{C}}}$.
$\mathbf{H}$	The channel matrix.
$\mathbf{n}$	The noise matrix.
E_{av}	The average energy of a M-ary E3D constellation.
$E_{\mathrm{av}}^{\Lambda}$	The average energy per TSV in the Λ system.
$\mathbf{X}$	The spatial vector modulating the component $S_{\mathrm{3D},x}$ of S_{3D} on one out of $\frac{N_{\mathrm{t}}}{2}$ (1-st,$\cdots$, $\frac{N_{\mathrm{t}}}{2}$-th) antennas.
$\bar{\mathbf{X}}$	The spatial vector modulating the component $S_{\mathrm{3D},x}$ of S_{3D} on one out of $\frac{N_{\mathrm{t}}}{2}$ ($\frac{N_{\mathrm{t}}}{2}+1\cdots$, N_{t}-th) antennas.
$\mathbf{Y}$	The spatial vector modulating the components $S_{\mathrm{3D},y}$, $S_{\mathrm{3D},z}$ of S_{3D} on two out of $\frac{N_{\mathrm{t}}}{2}$ (1-st,$\cdots$, $\frac{N_{\mathrm{t}}}{2}$-th) antennas.
$\bar{\mathbf{Y}}$	The spatial vector modulating the component $S_{\mathrm{3D},y}, S_{\mathrm{3D},z}$ of S_{3D} on two out of $\frac{N_{\mathrm{t}}}{2}$ ($\frac{N_{\mathrm{t}}}{2}+1\cdots$, N_{t}-th) antennas.
$\mathbf{V}$, $\tilde{\mathbf{V}}$	Two formations of the TSV.
$\bar{d}^2_{\mathbf{S},\min}$	Squared minimum Euclidean distance
C_a^b	Number of combinations of choosing b out of a elements.

III. INTRODUCTION

Multiple-input multiple-output (MIMO) technology can significantly enhance reliability and throughput of wireless communications with modest transmission power and system bandwidth, thanks to the achievable spatial multiplexing and diversity gains. The spatial multiplexing transmission schemes, such as the vertical Bell Labs layered space-time (V-BLAST) [1], satisfy the ever-increasing user demands for high data rates and have been applied for mobile communications base station with large-scale transmit antennas.

However, due to the strong co-channel interferences (CCI) in spatial multiplexing systems, a highly concerned index modulation, which called as spatial modulation (SM) [2]–[4], is proposed for relaxing the CCI by exploiting the third spatial domain. In SM system, the data information bits transmitted are divided into two blocks, one of which is carried by the conventional Quadrature Amplitude Modulation/Phase Shift Keying (QAM/PSK) signal constellation and the other one of which is carried by the spatial antenna indexes (AIes) of active transmit antennas. Subsequently, the active AI technique used to convey information bits have been attracted the attention of the researchers in the field of wireless communication. In order to exploit the AI information bits through the resource of transmit antennas, the extended techniques of SM reported in [5]–[12] are proposed to improve the spectral efficiency and enhance the bit error rate (BER) performance. In [5]–[8], the space shift keying (SSK) techniques are proposed for BER performance enhancement, while at the same time reducing the detection complexity. Furthermore, in order to achieve higher transmit rates and better BER performance than SM, the generalizing of SM, called as generalized spatial modulation (GSM) [9]–[12], activates simultaneously multiple transmit antennas to transmit different QAM/PSK symbols and increases the active AI combinations for conveying more AI information bits. Based on considering the real and imaginary dimensions in signal constellation domain, quadrature spatial modulation (QSM) [13] is proposed to improve SM/SSK's data rate and BER performance by extending the spatial dimension produced by active AI combinations to the in-phase and quadrature spatial dimensions that are respectively used to modulate the real and imaginary parts of a complex QAM/PSK symbol. In [14], inspired by QSM, the spatial constellation of SM is expanded to a new multi-dimensional constellations for the improvement of the BER performance. In [15]–[17], the approaches are proposed to improve the BER performance of the GSM system, even more reducing the detection complexity. Furthermore, to further improve the spectral efficiency, with the aid of a rotation angle, double spatial modulation (DSM) [18] scheme directly superimposes two independent SM transmission vectors for the achievable BER performance.

However, based on the above-mentioned works, the combination of signal constellation design and active transmit antenna(s) is not considered for improving the spectral

efficiency and BER performance. In order to make full use of the resource from both transmit antennas and signal constellations to achieve the spatial gain from the spatial and signal constellation domains, enhanced spatial modulation (ESM) [19], [20] is proposed. Its core idea is to increase more AI combinations used to carry AI index bits by combing the variable number of active transmit antennas with the signal constellation design (e.g. Secondary QAM constellations are designed). Moreover, the minimum Euclidean distance (MED) between the transmitted spatial vectors (TSVs) for the ESM system is increased as compared with the conventional MIMO with index modulation (MIMO-IM) techniques at the same spectral efficiency. Furthermore, based on the extending of component dimensions in signal constellation domain, Quadrature index modulation with three dimensional constellation (QIM-TDC) [21], in which a new three dimension (3D) signal constellation is designed, is proposed to enhance the squared MED between the TSVs for further lowering the BER. In [22], with the design of both pulse amplitude modulation (PAM) combining with the sign j and signal QAM constellation, generalized spatial modulation with multi-index modulation (GSM-MIM) improves the spectral efficiency and the BER performance by exploiting the spatial gain. Subsequently, with the aid of two states of both 1 and j, spatial modulation with spatial constellation design (SM-SC) reported in [23] develops the group index domain to further carry more spatial index bits and designs multi-dimension signal constellations to enlarge the squared MED between the TSVs for further enhancing the reliability of communications.

In view of the core ideas of the previous works, in this paper a new design method, called as generalized quadrature index modulation (GQIM) framework, is proposed and further develops the spatial domain with the spatial constellation design to enhance the spectral efficiency and reliability of the MIMO-IM communications system.

The main contributions of this paper are as follows:

1) The GQIM framework with extended three dimension (E3D) constellation is structured by exploiting the spatial domain with the aid of the key and vector indications, which enhances the transmit data rate and the BER performance of the MIMO-IM system as compared with the previous developed systems such as QSM, QIM-TDC, SM-SC.
2) Based on the GQIM framework, the E3D constellations are designed by extending the 2D signal constellations.
3) With the aid of the key and vector indications, not only the TSVs is designed to transmit more extra information bits, but also two versions of a E3D symbol are transmitted for the achievable transmit diversity gain.
4) Under the same MIMO configuration of transmit antennas and transmit data rates, the proposed GQIM system is capable of achieving a lower BER performance than the previous developed spatial modulation systems such as QSM, ESM, SM-SC and so on, For instance, at 19 bits/s/Hz and $[N_t, N_r] = [16, 8]$, the GQIM system outperforms approximately 4.5 dB SNR gains over SM-SC, 16.5 dB over QSM at BER of 10^{-2}.

In addition, in maritime Mesh network communication, the shore-based station plays a key role in the improvement of spectral efficiency and reliability of wireless communication. Once the shore base station collapses, the Mesh network will be paralyzed. In order to enhance the reliability of communication system between the shore-based station with the ships having multiple transmit antennas, we will further research the GQIM system and apply it to the shore-based station with small-scale transmit antennas.

The remaining part of this paper is organized as follows. System model of the proposed GQIM system is introduced in Section IV, in which the transmitter and receiver of the proposed GQIM system is respectively introduced in Sections IV-A and IV-D, and the transmitted spatial vector and the extended signal constellation are respectively designed in Sections IV-B and IV-C. The performance analyses, including the spectral efficiency and bit error probability, the spatial index bits and detection complexity, are provided in Section V. Simulation results are discussed in Section VI and our conclusion are given in SectionVII.

IV. THE PROPOSED GQIM SYSTEM

In this section, the proposed GQIM system, which is described in Fig.1, aims at exploiting the spatial and diversity gains from the spatial and signal constellation domains. In this paper, the bit stream I_B are mapped into a TSV symbol $\bar{\mathbf{S}}$ that is a normalized spatial vector. Then, the TSV $\bar{\mathbf{S}}$ is transmitted to the receiver through the Antenna Index Modulator modules, the Modulator of converting 2D to 3D constellation, the Vector Combiners and three Key Controllers. In what following, the detailed design of the GQIM system is investigated.

A. TRANSMITTER DESIGN

In the proposed GQIM system, as described in Fig. 1, let us consider the framework of the GQIM system with N_t transmit antennas and N_r receive antennas. Assuming there are

$$I_B = I_s + I_{SI} \tag{1}$$

incoming information bits transmitted in one GQIM symbol duration, where we define $I_{SI} = I_k + I_V + I_{AI}$ as the spatial index bits and $I_{AI} = I_A + I_{\bar{A}} + I_B + I_{\bar{B}} + I_C + I_{\bar{C}}$. The bit stream I_B is divided into two blocks such as I_s, I_{SI}. Furthermore, the block of I_{SI} is divided into three subblocks such as I_{AI}, I_k, I_V. Note that I_s, I_{AI}, I_k, I_V denote the block of symbol index bit, the subblock of spatial antenna index bits, the subblock of key index bit and the subblock of vector index bit, respectively.

Specifically, as described in the transmitter of the GQIM system in Fig. 1, through the Modulator of converting 2D to 3D constellation, the block of I_s, including $\log_2 M$ information bits, is used to be mapped on an E3D signal constellation

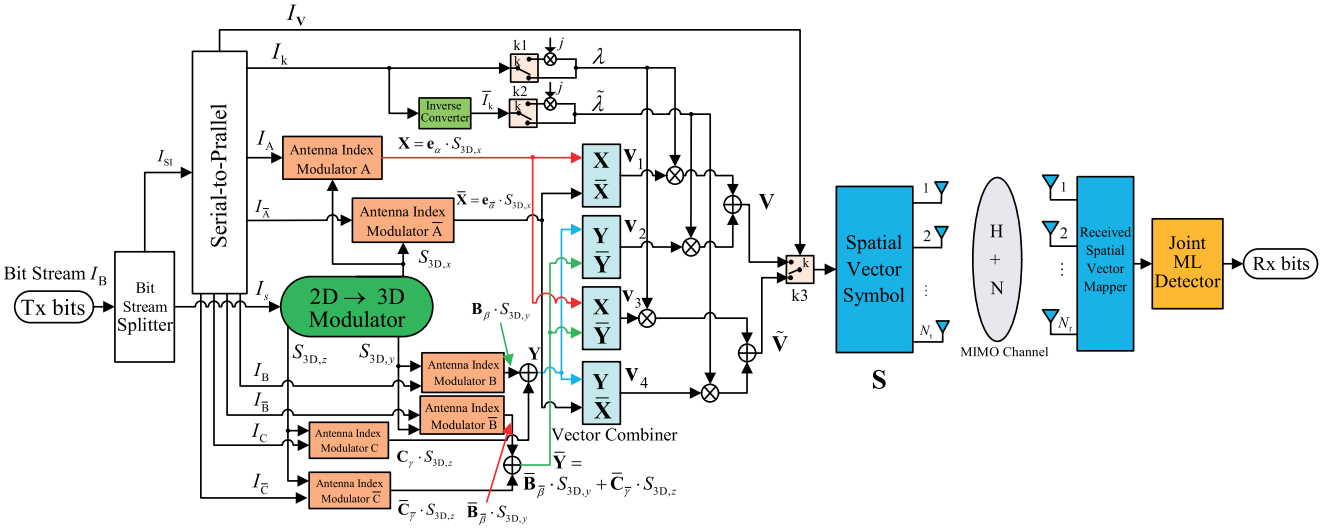

FIGURE 1. System model of GQIM structure.

point (CP) S_{3D} in a M-ary E3D constellation expressed by Λ, whose design details are provided in Section IV-C, where X-axis, Y-axis, Z-axis component values of the mapped E3D signal CP are respectively expressed by $S_{3D,x}, S_{3D,y}, S_{3D,z}$, M is the modulation order of the E3D signal constellation Λ. Then, in order to achieve the transmit diversity from the signal constellation domain, the mapped E3D signal CP S_{3D} is transformed into two versions that will be transmitted simultaneously on N_t transmit antennas without mutual interference. In other words, two versions of the mapped E3D symbol S_{3D} are respectively modulated on the first half (i.e., $1 \cdots, \frac{N_t}{2}$) of N_t transmit antennas through the Antenna Index Modulators of A, B, C and on the other half (i.e., $\frac{N_t}{2} + 1 \cdots, N_t$) of N_t transmit antennas through the Antenna Index Modulators $\bar{A}, \bar{B}, \bar{C}$. Thus, the transmitted spatial vectors (TSVs) including two identical versions of the mapped E3D symbol S_{3D} are transmitted to the receiver through N_t RF chains.

The subblock of I_{AI}, including $2 \cdot \log_2 \frac{N_t}{2} + 4 \cdot \log_2 \frac{N_t}{4}$ (i.e., $I_A + I_{\bar{A}} + I_B + I_{\bar{B}} + I_C + I_{\bar{C}}$) of spatial AI bits, are further divided into six subblocks that are respectively expressed by $I_A, I_{\bar{A}}, I_B, I_{\bar{B}}, I_C, I_{\bar{C}}$, each of which is used to select a specific AI combination vector of active transmit antennas for modulating one of three components $S_{3D,x}, S_{3D,y}, S_{3D,z}$ of the mapped E3D symbol S_{3D}. More specifically, the two subblocks of I_A and $I_{\bar{A}}$, each containing $\log_2 \frac{N_t}{2}$ bits, are respectively fed into the AI Modulator A for selecting an AI vector $\mathbf{e}_\alpha$ from the 1-st, $\cdots$, $\frac{N_t}{2}$-th column vectors of the AI vector set Ω_A and into the AI Modulator $\bar{A}$ for selecting an AI vector $\mathbf{e}_{\bar{\alpha}}$ from 1-st, $\cdots$, $\frac{N_t}{2}$-th column vectors of the AI vector set $\Omega_{\bar{A}}$. Note that, the AI vector set Ω_A, which may be equivalent to $\Omega_{\bar{A}}$, is similar to a $(\frac{N_t}{2} \times \frac{N_t}{2})$-element identity matrix $\mathbf{I}_{\frac{N_t}{2}}$ and expressed by

$$\Omega_A(\text{or } \Omega_{\bar{A}}) = \left[\mathbf{e}_1, \cdots, \mathbf{e}_{\alpha(\text{or } \bar{\alpha})}, \cdots, \mathbf{e}_{\frac{N_t}{2}}\right] = \begin{bmatrix} 1 & 0 & 0 & \cdots & 0 & 0 & 0 & 0 \\ 0 & 1 & 0 & \vdots & 0 & 0 & 0 & 0 \\ \vdots & 0 & 1 & 0 & \vdots & 0 & 0 & 0 \\ 0 & \vdots & 0 & \ddots & 0 & \vdots & 0 & 0 \\ 0 & 0 & \vdots & 0 & \ddots & 0 & \vdots & 0 \\ 0 & 0 & 0 & \vdots & 0 & 1 & 0 & \vdots \\ 0 & 0 & 0 & 0 & \vdots & 0 & 1 & 0 \\ 0 & 0 & 0 & \cdots & 0 & 0 & 0 & 1 \end{bmatrix}_{\frac{N_t}{2} \times \frac{N_t}{2}}, \quad (2)$$

where $\mathbf{e}_\alpha$ and $\mathbf{e}_{\bar{\alpha}}$ denote the α-th column vector of the vector set Ω_A and $\bar{\alpha}$-th column vector of the vector set $\Omega_{\bar{A}}$, respectively. Then, the selected AI vector $\mathbf{e}_\alpha$ and $\mathbf{e}_{\bar{\alpha}}$ are respectively modulate the component $S_{3D,x}$ from two versions of the mapped E3D symbol S_{3D}. Consequently, as shown in Fig. 1, the vector outputs of the AI Modulator A and $\bar{A}$ are respectively obtained as

$$\mathbf{X} = \mathbf{e}_\alpha \cdot S_{3D,x}, \quad \bar{\mathbf{X}} = \mathbf{e}_{\bar{\alpha}} \cdot S_{3D,x}. \quad (3)$$

Similarly, on the one hand, through two AI Modulators B and $\bar{B}$, the subblocks of I_B and $I_{\bar{B}}$, each containing $\log_2 \frac{N_t}{4}$ information bits, are used to select an AI vector $\mathbf{B}_\beta$ from the AI vector set Ω_B and to select an AI vector $\bar{\mathbf{B}}_{\bar{\beta}}$ from the AI set $\Omega_{\bar{B}}$, respectively, where $\beta, \bar{\beta} \in \left\{1, \cdots, \frac{N_t}{4}\right\}$ and the two AI vector sets $(\Omega_B, \Omega_{\bar{B}})$ will be provided later. Then, the vector output $\mathbf{B}_\beta \cdot S_{3D,y}$ of the AI Modulator B is obtained by using the AI vector $\mathbf{B}_\beta$ to modulate the component $S_{3D,y}$ from one version of the mapped E3D symbol S_{3D}. Also, the vector output $\bar{\mathbf{B}}_{\bar{\beta}} \cdot S_{3D,y}$ of the AI Modulator $\bar{B}$ is obtained by using the AI vector $\bar{\mathbf{B}}_{\bar{\beta}}$ to modulate $S_{3D,y}$ from the other version of the E3D symbol S_{3D}.

On the other hand, through two AI Modulators C and $\bar{C}$, the last two subblocks of I_C and $I_{\bar{C}}$, each containing $\log_2 \frac{N_t}{4}$

information bits, are respectively used to select an AI vector $\mathbf{C}_\gamma$ from the AI vector set Ω_{C} and to select an AI vector $\bar{\mathbf{C}}_{\bar{\gamma}}$ from the AI vector set $\Omega_{\bar{\mathrm{C}}}$, where $\gamma, \bar{\gamma} \in \left\{1, \cdots, \frac{N_\mathrm{t}}{4}\right\}$. Then, the obtained AI vector $\mathbf{C}_\gamma$ and $\bar{\mathbf{C}}_{\bar{\gamma}}$ are used to modulate the same component $S_{3\mathrm{D},z}$ from two versions of the E3D symbol $S_{3\mathrm{D}}$, resulting in the vector symbol $\mathbf{C}_\gamma \cdot S_{3\mathrm{D},z}$ and the vector symbol $\bar{\mathbf{C}}_{\bar{\gamma}} \cdot S_{3\mathrm{D},z}$, respectively.

It is very important to note that $\mathbf{B}_\beta \cdot S_{3\mathrm{D},y}$ and $\mathbf{C}_\gamma \cdot S_{3\mathrm{D},z}$ are transmitted on the first half (i.e., the 1-st,$\cdots$, $\frac{N_\mathrm{t}}{2}$-th antennas) of N_t transmit antennas, but $\bar{\mathbf{B}}_{\bar{\beta}} \cdot S_{3\mathrm{D},y}$ and $\bar{\mathbf{C}}_{\bar{\gamma}} \cdot S_{3\mathrm{D},z}$ are transmitted on the other half (i.e., the $\frac{N_\mathrm{t}}{2}+1 \cdots$, N_t-th antennas) of N_t transmit antennas. However, if the $\mathbf{B}_\beta$, $\bar{\mathbf{B}}_{\bar{\beta}}$ and $\mathbf{C}_\gamma$, $\bar{\mathbf{C}}_{\bar{\gamma}}$ are not well designed, the two components $S_{3\mathrm{D},y}$ and $S_{3\mathrm{D},z}$ from the mapped E3D symbol $S_{3\mathrm{D}}$ may be overlapped in the process of forming a TSV operation. It will lead to produce the higher bit error ratio at the detection of the receiver. To solving this problem, the aforementioned AI vector set Ω_{B} being equivalent to $\Omega_{\bar{\mathrm{B}}}$, Ω_{C} being equivalent to $\Omega_{\bar{\mathrm{C}}}$ may be respectively designed as

$$\Omega_{\mathrm{B}} = \left[\mathbf{B}_1, \cdots, \mathbf{B}_\beta, \cdots, \mathbf{B}_{\frac{N_\mathrm{t}}{4}}\right] = \begin{bmatrix} 1 & 0 & \cdots & 0 \\ 0 & 1 & 0 & \vdots \\ \vdots & 0 & \ddots & 0 \\ 0 & \vdots & 0 & 1 \\ 0 & 0 & 0 & 0 \\ 0 & 0 & 0 & 0 \\ 0 & 0 & 0 & 0 \\ 0 & 0 & 0 & 0 \end{bmatrix}_D$$

$$\Omega_{\mathrm{C}} = \left[\mathbf{C}_1, \cdots, \mathbf{C}_\gamma, \cdots, \mathbf{C}_{\frac{N_\mathrm{t}}{4}}\right] = \begin{bmatrix} 0 & 0 & 0 & 0 \\ 0 & 0 & 0 & 0 \\ 0 & 0 & 0 & 0 \\ 0 & 0 & 0 & 0 \\ 1 & 0 & 0 & 0 \\ 0 & 1 & 0 & \vdots \\ \vdots & \ddots & \ddots & 0 \\ 0 & 0 & 0 & 1 \end{bmatrix}_D, \quad (4)$$

where the parameter D in (4) denotes $\frac{N_\mathrm{t}}{2} \times \frac{N_\mathrm{t}}{4}$.

Thus, a spatial vector $\mathbf{Y}$, which combining with the spatial vector $\mathbf{X}$ will be modulated on the 1-st, $\cdots$, $\frac{N_\mathrm{t}}{2}$-th transmit antennas, is obtained by adding the vector symbol $\mathbf{B}_\beta \cdot S_{3\mathrm{D},y}$ and the vector symbol $\mathbf{C}_\gamma \cdot S_{3\mathrm{D},z}$, as follows

$$\mathbf{Y} = \mathbf{B}_\beta \cdot S_{3\mathrm{D},y} + \mathbf{C}_\gamma \cdot S_{3\mathrm{D},z}. \quad (5)$$

Similarly, by adding the vector symbol $\bar{\mathbf{B}}_{\bar{\beta}} \cdot S_{3\mathrm{D},y}$ and the vector symbol $\bar{\mathbf{C}}_{\bar{\gamma}} \cdot S_{3\mathrm{D},z}$, the spatial vector $\bar{\mathbf{Y}}$, which combining with the spatial vector $\bar{\mathbf{X}}$ will be modulated on the $\frac{N_\mathrm{t}}{2}+1, \cdots$, N_t-th transmit antennas, is obtained as

$$\bar{\mathbf{Y}} = \bar{\mathbf{B}}_{\bar{\beta}} \cdot S_{3\mathrm{D},y} + \bar{\mathbf{C}}_{\bar{\gamma}} \cdot S_{3\mathrm{D},z}. \quad (6)$$

For further explain the working principle of generating the spatial vectors (e.g. $\mathbf{X}$, $\bar{\mathbf{X}}$, $\mathbf{Y}$, $\bar{\mathbf{Y}}$), examples showing the values of the above-mentioned variables with the spatial AI information bits

$$I_{\mathrm{AI}} = \left[\underbrace{b_1, b_2}_{I_{\mathrm{A}}}, \underbrace{b_3, b_4}_{I_{\bar{\mathrm{A}}}}, \underbrace{b_5}_{I_{\mathrm{B}}}, \underbrace{b_6}_{I_{\bar{\mathrm{B}}}}, \underbrace{b_7}_{I_{\mathrm{C}}}, \underbrace{b_8}_{I_{\bar{\mathrm{C}}}}\right]$$

and $N_\mathrm{t} = 8$ are provided in Table 1. Assumed that a mapped E3D signal CP symbol S_{E3D} with $S_{3\mathrm{D},x}, S_{3\mathrm{D},y}, S_{3\mathrm{D},z}$, $\Omega_{\mathrm{A}} = \Omega_{\bar{\mathrm{A}}} = \{[1\ 0\ 0\ 0]^T, [0\ 1\ 0\ 0]^T, [0\ 0\ 1\ 0]^T, [0\ 0\ 0\ 1]^T\}$, $\Omega_{\mathrm{B}} = \Omega_{\bar{\mathrm{B}}} = \left\{[1\,0\,0\,0]^T, [0\,1\,0\,0]^T\right\}$, $\Omega_{\mathrm{C}} = \Omega_{\bar{\mathrm{C}}} = \left\{[0\,0\,1\,0]^T, [0\,0\,0\,1]^T\right\}$, where 0 and 1 denotes the off and on of the corresponding transmit antenna, respectively. The detailed results are shown in TABLE 1.

Based on the above mentioned design of the proposed GQIM system, the above obtained spatial vectors $\mathbf{X}$, $\mathbf{Y}$ are transmitted on 1-st, $\cdots$, $\frac{N_\mathrm{t}}{2}$-th transmit antennas and the above obtained spatial vectors $\bar{\mathbf{X}}$, $\bar{\mathbf{Y}}$ are transmitted on $\frac{N_\mathrm{t}}{2} + 1 \cdots$, N_t-th transmit antennas. Hence, through the Vector Combiners, the above spatial vectors (e.g. $\mathbf{X}$, $\bar{\mathbf{X}}$, $\mathbf{Y}$, $\bar{\mathbf{Y}}$,) are combined into four cases of spatial vectors, which are respectively given by

$$\mathbf{v}_1 = \begin{bmatrix} \mathbf{X} \\ \bar{\mathbf{X}} \end{bmatrix}, \quad \mathbf{v}_2 = \begin{bmatrix} \mathbf{Y} \\ \bar{\mathbf{Y}} \end{bmatrix}, \ \mathbf{v}_3 = \begin{bmatrix} \mathbf{X} \\ \bar{\mathbf{Y}} \end{bmatrix}, \ \mathbf{v}_4 = \begin{bmatrix} \mathbf{Y} \\ \bar{\mathbf{X}} \end{bmatrix}. \quad (7)$$

Obviously, as shown in Fig. 1, in order to be capable of simultaneously transmitting the two versions of a E3D symbol with N_t transmit antennas, the complex TSV $\mathbf{S}$ is obtained by combining the spatial vector $\mathbf{v}_1$ with the spatial vector $\mathbf{v}_2$, or by combining the spatial vector $\mathbf{v_3}$ with the spatial vector $\mathbf{v}_4$. In order to further achieve the higher spectral efficiency, the real and imaginary parts of the complex TSV $\mathbf{S}$ need a flexible selection with the two Key Controller.

Furthermore, with the aid of the two Key Control Modules, each of which controls two states of both "1" and "j" and which are used for data transmission, one more index bit is transmitted for enhancing the spectral efficiency of system. Specifically, the block of I_k containing "1" bit, is used to control the two keys for determining the real and imaginary parts of the complex TSV. On the one hand, a key $\mathbf{k1}$ is directly controlled by the index bit I_k. Thus, the expression of the relation between the output λ and the input I_k of the $\mathbf{k1}$ module is given by

$$\lambda = \begin{cases} 1, & I_\mathrm{k} = 0 \\ j, & I_\mathrm{k} = 1, \end{cases} \quad (8)$$

where $j = \sqrt{-1}$. According to the index bit I_k, the resulted output λ value then multiplies by the spatial vector $\mathbf{v_1}$ for the derivation of $\mathbf{v_1} \cdot \lambda$ and by the spatial vector $\mathbf{v_3}$ for the derivation of $\mathbf{v_3} \cdot \lambda$.

On the other hand, through the Inverse Converter, the block of I_k index bit is converted into the inverse value $\bar{I}_\mathrm{k}$. Furthermore, the value $\bar{I}_\mathrm{k}$ is used to control the key $\mathbf{k2}$. Such that the relation between the output $\tilde{\lambda}$ and the input I_k of the

TABLE 1. Using the spatial index bits $I_{\mathrm{AI}} = 8$ (i.e., $I_{\mathrm{A}}, I_{\bar{\mathrm{A}}}, I_{\mathrm{B}}, I_{\bar{\mathrm{B}}}, I_{\mathrm{C}}, I_{\bar{\mathrm{C}}}$) and $N_{\mathrm{t}} = 8$ transmit antennas, examples of generating the spatial vectors, which are obtained by modulating a E3D symbol S_{3D} ($S_{\mathrm{3D},x}, S_{\mathrm{3D},y}, S_{\mathrm{3D},z}$) on the active transmit antennas, are provided.

I_{AI} bits	Antenna Index Vector						Spatial Vectors			
I_{A}	$\mathbf{e}_\alpha$	$\mathbf{e}_{\bar{\alpha}}$	$\mathbf{B}_\beta$	$\mathbf{B}_{\bar{\beta}}$	$\mathbf{C}_\gamma$	$\mathbf{C}_{\bar{\gamma}}$	$\mathbf{X}$	$\bar{\mathbf{X}}$	$\mathbf{Y}$	$\bar{\mathbf{Y}}$
00000101	$\mathbf{e}_1$	$\mathbf{e}_1$	$\mathbf{B}_1$	$\bar{\mathbf{B}}_2$	$\mathbf{C}_1$	$\bar{\mathbf{C}}_2$	$\mathbf{e}_1 \cdot S_{\mathrm{3D},x}$	$\mathbf{e}_1 \cdot S_{\mathrm{3D},x}$	$\mathbf{B}_1 \cdot S_{\mathrm{3D},y} + \mathbf{C}_1 \cdot S_{\mathrm{3D},z}$	$\bar{\mathbf{B}}_2 \cdot S_{\mathrm{3D},y} + \bar{\mathbf{C}}_2 \cdot S_{\mathrm{3D},z}$
00011100	$\mathbf{e}_1$	$\mathbf{e}_2$	$\mathbf{B}_2$	$\bar{\mathbf{B}}_2$	$\mathbf{C}_1$	$\bar{\mathbf{C}}_1$	$\mathbf{e}_1 \cdot S_{\mathrm{3D},x}$	$\mathbf{e}_2 \cdot S_{\mathrm{3D},x}$	$\mathbf{B}_2 \cdot S_{\mathrm{3D},y} + \mathbf{C}_1 \cdot S_{\mathrm{3D},z}$	$\bar{\mathbf{B}}_2 \cdot S_{\mathrm{3D},y} + \bar{\mathbf{C}}_1 \cdot S_{\mathrm{3D},z}$
01000101	$\mathbf{e}_2$	$\mathbf{e}_1$	$\mathbf{B}_1$	$\bar{\mathbf{B}}_2$	$\mathbf{C}_1$	$\bar{\mathbf{C}}_2$	$\mathbf{e}_2 \cdot S_{\mathrm{3D},x}$	$\mathbf{e}_1 \cdot S_{\mathrm{3D},x}$	$\mathbf{B}_1 \cdot S_{\mathrm{3D},y} + \mathbf{C}_1 \cdot S_{\mathrm{3D},z}$	$\bar{\mathbf{B}}_2 \cdot S_{\mathrm{3D},y} + \bar{\mathbf{C}}_2 \cdot S_{\mathrm{3D},z}$
01011110	$\mathbf{e}_2$	$\mathbf{e}_2$	$\mathbf{B}_2$	$\bar{\mathbf{B}}_2$	$\mathbf{C}_2$	$\bar{\mathbf{C}}_1$	$\mathbf{e}_2 \cdot S_{\mathrm{3D},x}$	$\mathbf{e}_2 \cdot S_{\mathrm{3D},x}$	$\mathbf{B}_2 \cdot S_{\mathrm{3D},y} + \mathbf{C}_2 \cdot S_{\mathrm{3D},z}$	$\bar{\mathbf{B}}_2 \cdot S_{\mathrm{3D},y} + \bar{\mathbf{C}}_1 \cdot S_{\mathrm{3D},z}$
10100111	$\mathbf{e}_3$	$\mathbf{e}_3$	$\mathbf{B}_1$	$\bar{\mathbf{B}}_2$	$\mathbf{C}_2$	$\bar{\mathbf{C}}_2$	$\mathbf{e}_3 \cdot S_{\mathrm{3D},x}$	$\mathbf{e}_3 \cdot S_{\mathrm{3D},x}$	$\mathbf{B}_1 \cdot S_{\mathrm{3D},y} + \mathbf{C}_2 \cdot S_{\mathrm{3D},z}$	$\bar{\mathbf{B}}_2 \cdot S_{\mathrm{3D},y} + \bar{\mathbf{C}}_2 \cdot S_{\mathrm{3D},z}$
10111000	$\mathbf{e}_3$	$\mathbf{e}_4$	$\mathbf{B}_2$	$\bar{\mathbf{B}}_1$	$\mathbf{C}_1$	$\bar{\mathbf{C}}_1$	$\mathbf{e}_3 \cdot S_{\mathrm{3D},x}$	$\mathbf{e}_4 \cdot S_{\mathrm{3D},x}$	$\mathbf{B}_2 \cdot S_{\mathrm{3D},y} + \mathbf{C}_1 \cdot S_{\mathrm{3D},z}$	$\bar{\mathbf{B}}_1 \cdot S_{\mathrm{3D},y} + \bar{\mathbf{C}}_1 \cdot S_{\mathrm{3D},z}$
11001001	$\mathbf{e}_4$	$\mathbf{e}_1$	$\mathbf{B}_2$	$\bar{\mathbf{B}}_1$	$\mathbf{C}_1$	$\bar{\mathbf{C}}_2$	$\mathbf{e}_4 \cdot S_{\mathrm{3D},x}$	$\mathbf{e}_1 \cdot S_{\mathrm{3D},x}$	$\mathbf{B}_2 \cdot S_{\mathrm{3D},y} + \mathbf{C}_1 \cdot S_{\mathrm{3D},z}$	$\bar{\mathbf{B}}_1 \cdot S_{\mathrm{3D},y} + \bar{\mathbf{C}}_2 \cdot S_{\mathrm{3D},z}$
11011010	$\mathbf{e}_4$	$\mathbf{e}_2$	$\mathbf{B}_2$	$\bar{\mathbf{B}}_1$	$\mathbf{C}_2$	$\bar{\mathbf{C}}_1$	$\mathbf{e}_4 \cdot S_{\mathrm{3D},x}$	$\mathbf{e}_2 \cdot S_{\mathrm{3D},x}$	$\mathbf{B}_2 \cdot S_{\mathrm{3D},y} + \mathbf{C}_2 \cdot S_{\mathrm{3D},z}$	$\bar{\mathbf{B}}_1 \cdot S_{\mathrm{3D},y} + \bar{\mathbf{C}}_1 \cdot S_{\mathrm{3D},z}$

k2 module is as follows

$$\tilde{\lambda} = \begin{cases} 1, & I_{\mathrm{k}} = 1 \\ j, & I_{\mathrm{k}} = 0. \end{cases} \tag{9}$$

According to the index bit I_{k}, the resulted output $\tilde{\lambda}$ value then multiplies by the spatial vector $\mathbf{v_2}$ for the derivation of $\mathbf{v_2} \cdot \tilde{\lambda}$ and by the spatial vector $\mathbf{v_4}$ for the derivation of $\mathbf{v_4} \cdot \tilde{\lambda}$.

B. TRANSMITTED SPATIAL VECTOR

Based on the above design and analysis, through two Vector Adder depicted in Fig. 1, we obtain two formations about the complex TSV $\mathbf{S}$, which are given by

$$\begin{aligned} \mathbf{V} &= \mathbf{v}_1 \cdot \lambda + \mathbf{v}_2 \cdot \tilde{\lambda} = \begin{bmatrix} \mathbf{X} \\ \bar{\mathbf{X}} \end{bmatrix} \cdot \lambda + \begin{bmatrix} \mathbf{Y} \\ \bar{\mathbf{Y}} \end{bmatrix} \cdot \tilde{\lambda} \\ \tilde{\mathbf{V}} &= \mathbf{v}_3 \cdot \lambda + \mathbf{v}_4 \cdot \tilde{\lambda} = \begin{bmatrix} \mathbf{X} \\ \bar{\mathbf{Y}} \end{bmatrix} \cdot \lambda + \begin{bmatrix} \mathbf{Y} \\ \bar{\mathbf{X}} \end{bmatrix} \cdot \tilde{\lambda}. \end{aligned} \tag{10}$$

Thus, it provides two options for the complex TSV $\mathbf{S}$.

Finally, due to that there existing two formations of the TSV $\mathbf{S}$, one more index bit can be also transmitted for enhancing the spectral efficiency of system. In this paper, we use the block of $I_{\mathbf{V}}$ containing "1" information bit to determine a TSV symbol $\mathbf{S}$ from the TSV set $\Omega_{\mathbf{S}} = \{\mathbf{V}, \tilde{\mathbf{V}}\}$ obtained by (10), which is expressed by

$$\mathbf{S} = \begin{cases} \mathbf{V}, & \zeta = 1 \\ \tilde{\mathbf{V}}, & \zeta = 2, \end{cases} \tag{11}$$

where $\zeta \in \{1,\ 2\}$ is the statement of the TSV indication for the vector index bit $I_{\mathbf{V}}$.

To further explain the working principle of creating a complex TSV $\mathbf{S}$, examples are given in what follows. Assumed that $N_{\mathrm{t}} = 8$, based on the results of Table 1 and (7), (8), (9), (10), (11), the TSVs are generated as the results shown in Table 2.

C. DESIGN OF EXTENDED SIGNAL CONSTELLATION

In the M-ary E3D (2D to 3D) constellation modulator portrayed in Fig. 1, whose details are provided in Fig. 2, based on the above design, the block of I_s bits is mapped into one E3D signal CP $S_{\mathrm{3D}}(S_{\mathrm{3D},x}, S_{\mathrm{3D},y}, S_{\mathrm{3D},z})$ of the mapped E3D constellation Λ. Specifically, as shown in the left of Fig. 2, the I_s number of input bits are split into two subblocks, where we define $I_s = I_{\mathrm{C}} + I_\varepsilon = \log_2 N + 1$. The first subblock of $I_{\mathrm{C}} = \log_2 N$ bits is used to select a signal CP symbol s from a given N-ary 2D signal constellation. The second subblock only contains $I_\varepsilon = 1$ bit, which is the sign indication bit that is used to select a sign χ from the set $\Gamma = \{1, -1\}$.

Before elaborating further on Fig. 2, the different from the target of conventional constellation design is pointed out that our proposed E3D signal constellation design aims to maximise the MED between the TSVs at the same transmit rate. In other words, although the squared MED of the E3D constellation may not be larger than that of 2D signal constellations with the same order, we ensure that the squared MED between the TSVs is larger in the GQIM system than in the existing classic spatial modulation variants. Let us now use Fig. 2 to explain how to construct a good TSV.

Firstly, the signal constellation symbol s is fed into the real/imaginary component comparison module observed in Fig. 2. Then, through the real/imaginary component comparison, the outputs have $s_{\max}$ and $s_{\min}$, which are given by

$$\begin{aligned} &\begin{cases} s_{\max} = \mathrm{sgn}\,(\Upsilon) \cdot \delta_{\max} \\ s_{\min} = \mathrm{sgn}(\tilde{\Upsilon}) \cdot \delta_{\min} \end{cases} \\ &\Upsilon = \begin{cases} s_\Re & \text{if } |s_\Re| \geq |s_\Im| \\ s_\Im & \text{if } |s_\Re| < |s_\Im| \end{cases} \\ &\tilde{\Upsilon} = \begin{cases} s_\Im & \text{if } |s_\Re| \geq |s_\Im| \\ s_\Re & \text{if } |s_\Re| < |s_\Im|, \end{cases} \end{aligned} \tag{12}$$

where $\delta_{\max} = \max\left\{|s_\Re|, |s_\Im|\right\}$, $\delta_{\min} = \min\left\{|s_\Re|, |s_\Im|\right\}$, and $\mathrm{sgn}(x)$ is the function to get the sign of x, while $s_\Re$ and $s_\Im$ are the real and imaginary parts of the N-ary 2D signal constellation symbol s, as observed at the top-left part of Fig. 2. Furthermore, according to Fig. 2, we need to construct two rotated versions of $s_{\max}$, namely $S_{\mathrm{3D},\mu} = s_{\max}^{\cos} = s_{\max} \cdot \cos\theta$ and $S_{\mathrm{3D},\nu} = s_{\max}^{\sin} = s_{\max} \cdot \sin\theta$ with the aid of the angle θ that is analyzed and provided later, where $\mu, \nu \in \{x, y, z\}$. It is very important to note that $s_{\max}^{\cos}$ and $s_{\max}^{\sin}$ always have the same sign, which is not in favour of MED maximisation. Hence, we use one additional index bit I_ε to randomise the sign of $s_{\max}^{\sin}$ or $s_{\max}^{\cos}$, resulting in $\chi \cdot s_{\max}^{\sin}$ or $\chi \cdot s_{\max}^{\cos}$. If one of both $\chi \cdot s_{\max}^{\sin}$ and $\chi \cdot s_{\max}^{\cos}$ is considered to construct a E3D

TABLE 2. Examples of generating a complex TSV symbol with the key index bit I_{k} and the vector index bit $I_{\mathbf{V}}$ at one time slot.

Key and Vector Index Bits		Output of Key Controller		TSV Indication	Spatial Vector		TSV
I_{k}	$I_{\mathbf{V}}$	λ	$\tilde{\lambda}$	ζ	$\mathbf{V}$	$\tilde{\mathbf{V}}$	$\mathbf{S}$
0	0	1	j	1	$\mathbf{v}_1+\mathbf{v}_2\cdot j$	$\mathbf{v}_3+\mathbf{v}_4\cdot j$	$\mathbf{v}_1+\mathbf{v}_2\cdot j$
0	1	1	j	2	$\mathbf{v}_1+\mathbf{v}_2\cdot j$	$\mathbf{v}_3+\mathbf{v}_4\cdot j$	$\mathbf{v}_3+\mathbf{v}_4\cdot j$
1	0	j	1	1	$\mathbf{v}_1\cdot j+\mathbf{v}_2$	$\mathbf{v}_3\cdot j+\mathbf{v}_4$	$\mathbf{v}_1\cdot j+\mathbf{v}_2$
1	1	j	1	2	$\mathbf{v}_1\cdot j+\mathbf{v}_2$	$\mathbf{v}_3\cdot j+\mathbf{v}_4$	$\mathbf{v}_3\cdot j+\mathbf{v}_4$

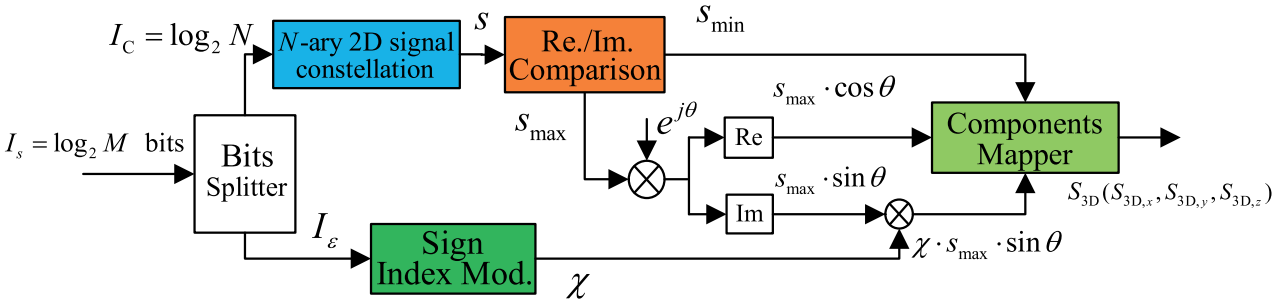

FIGURE 2. The M-ary E3D constellation mapping procedure.

symbol, it implies a total of 6 combinations as follows

$$S_{3\mathrm{D}}=\left(S_{3\mathrm{D},x},S_{3\mathrm{D},y},S_{3\mathrm{D},z}\right)=\begin{cases}\left(s_{\max}^{\cos},\chi\cdot s_{\max}^{\sin},s_{\min}\right) & (a)\\ \left(s_{\max}^{\sin},\chi\cdot s_{\max}^{\cos},s_{\min}\right) & (b)\\ \left(s_{\max}^{\cos},s_{\min},\chi\cdot s_{\max}^{\sin}\right) & (c)\\ \left(s_{\max}^{\sin},s_{\min},\chi\cdot s_{\max}^{\cos}\right) & (d)\\ \left(s_{\min},s_{\max}^{\cos},\chi\cdot s_{\max}^{\sin}\right) & (e)\\ \left(s_{\min},s_{\max}^{\sin},\chi\cdot s_{\max}^{\cos}\right) & (f)\end{cases}. \tag{13}$$

However, some of these combinations in (13) may lead to the same TSV even given different symbols $S_{3\mathrm{D}}$, depending on the above mentioned specific AI vectors (e.g. $\mathbf{e}_\alpha$, $\mathbf{e}_{\bar{\alpha}}$, $\mathbf{B}_\beta$, $\bar{\mathbf{B}}_{\bar{\beta}}$, $\mathbf{C}_\gamma$, $\bar{\mathbf{C}}_{\bar{\gamma}}$). For instance, assumed that $\theta=\frac{\pi}{4}$, $\chi=1$, according to two cases of (a), (b) in (13), due to the equality of $\cos\theta=\sin\theta$, it has $(s_{\max}^{\cos},\chi\cdot s_{\max}^{\sin},s_{\min})=(s_{\max}^{\sin},\chi\cdot s_{\max}^{\cos},s_{\min})$. Consequently, this will cause unrecoverable detection errors at the receiver. Hence, we only consider this case of $\chi\cdot s_{\max}^{\sin}$ in this paper, as exemplified in the bottom-right part of Fig. 2. Thus, we then have three components $s_{\max}^{\cos}$, $\chi\cdot s_{\max}^{\sin}$ and $s_{\min}$ to be used as three coordinates of the E3D symbol $S_{3\mathrm{D}}$, i.e., $(S_{3\mathrm{D},x},S_{3\mathrm{D},y},S_{3\mathrm{D},z})$. In (13), (a), (c) and (e) may be three legitimate cases. Moreover, by considering the absolute value comparison between $|s_{\Re}|$ and $|s_{\Im}|$, the output E3D symbol $S_{3\mathrm{D}}$ of the Components Mapper may be given by

$$S_{3\mathrm{D}}=\left(S_{3\mathrm{D},x},S_{3\mathrm{D},y},S_{3\mathrm{D},z}\right)=\begin{cases}\left(s_{\max}^{\cos},\chi\cdot s_{\max}^{\sin},s_{\min}\right) & \text{if } |s_{\Re}|>|s_{\Im}|\\ \left(s_{\min},s_{\max}^{\cos},\chi\cdot s_{\max}^{\sin}\right) & \text{if } |s_{\Re}|<|s_{\Im}|\\ \left(s_{\max}^{\cos},s_{\min},\chi\cdot s_{\max}^{\sin}\right) & \text{if } |s_{\Re}|=|s_{\Im}|.\end{cases} \tag{14}$$

Based on the above design, it should note that $\left|s_{\max}^{\cos}\right|$ or $\left|s_{\max}^{\sin}\right|$ may be smaller than $|s_{\min}|$. Due to the decreasing of the squared MED, it will lower the BER performance. To enhancing the squared MED between the TSVs, we need to analyze the squared MED between TSVs and design the rotating angle θ. According to the TSV symbol $\mathbf{S}$ obtained in (10) and (11), the squared MED between the normalized TSVs may be calculated by

$$\begin{aligned}\bar{d}^2_{\mathbf{S},\min}&=\min_{\omega\neq\bar{\omega}}\left\{\left\|\frac{\mathbf{S}_\omega}{\sqrt{2\cdot E_{\mathrm{av}}}}-\frac{\mathbf{S}_{\bar{\omega}}}{\sqrt{2\cdot E_{\mathrm{av}}}}\right\|^2\right\}\\&=\min_{\omega\neq\bar{\omega}}\left\{\left\|\bar{\mathbf{S}}_\omega-\bar{\mathbf{S}}_{\bar{\omega}}\right\|^2\right\}\\&=\min_{\omega\neq\bar{\omega}}\left\{\frac{|S_{3\mathrm{D},x}|^2}{E_{\mathrm{av}}},\frac{|S_{3\mathrm{D},y}|^2}{E_{\mathrm{av}}},\frac{|S_{3\mathrm{D},z}|^2}{E_{\mathrm{av}}}\right\}\\&=\min_{\omega\neq\bar{\omega}}\left\{\frac{|s_{\min}|^2}{E_{\mathrm{av}}},\frac{|s_{\max}^{\cos}|^2}{E_{\mathrm{av}}},\frac{|s_{\min}^{\sin}|^2}{E_{\mathrm{av}}}\right\},\end{aligned} \tag{15}$$

where $\bar{\mathbf{S}}=\frac{\mathbf{S}}{\sqrt{2\cdot E_{\mathrm{av}}}}$ denotes the normalized spatial vector corresponding to the TSV symbol $\mathbf{S}$, E_{av} denotes the average energy of each constellation point in a M-ary E3D constellation.

Nevertheless, in conventional 2D QAM signal constellation, its constellation point has the component values $|s_{\min}|=|s_{\max}|=1$. To enhance the TSV's MED after rotation of angle, it needs to satisfy $\frac{|\cos\theta|^2}{E_{\mathrm{av}}}=\frac{|\sin\theta|^2}{E_{\mathrm{av}}}$. Then, the rotation angle θ is designed as $\theta=\frac{\pi}{4}$. Consequently, combining with (14) and (15), the squared MED of GQIM has $\bar{d}^2_{\mathbf{S},\min}=\min\left\{\frac{|\cos\theta|^2}{E_{\mathrm{av}}},\frac{|\sin\theta|^2}{E_{\mathrm{av}}}\right\}$. Thus, $\bar{d}^2_{\mathbf{S},\min}$ may be rewritten as follows

$$\bar{d}^2_{\mathbf{S},\min}=\frac{1}{2\cdot E_{\mathrm{av}}}. \tag{16}$$

For the 2D PSK constellation, since QPSK is equivalent to 4QAM and high-order PSK constellation is

not good as high-order QAM constellation in terms of the MED, here we only consider the 8PSK constellation. In the 8PSK constellation such as $8\text{PSK} = \left\{ \begin{matrix} -0.3827-0.9239i, -0.9239-0.3827i, \\ -0.3827+0.9239i, -0.9239+0.3827i \\ 0.3827-0.9239i, 0.9239-0.3827i, \\ 0.3827+0.9239i, 0.9239+0.3827i \end{matrix} \right\}$, in order to enhance the TSV's MED and satisfy $|s_{\min}| \leq \left|s_{\max}^{\cos}\right|, |s_{\min}| \leq \left|s_{\max}^{\sin}\right|^2$, the range of rotation angle θ for 8PSK is designed as $\arcsin \frac{0.3827}{0.9239} \leq \theta \leq \arccos \frac{0.3827}{0.9239}$. Thus, the rotation angle is also designed as $\theta = \frac{\pi}{4}$. On account of $E_{\text{av}} = 1$ in the 2D PSK constellation, $\bar{d}^2_{\mathbf{S},\min}$ of (15) may be rewritten as follows

$$\bar{d}^2_{\mathbf{S},\min} = |s_{\min}|^2 . \tag{17}$$

D. RECEIVER

In this paper, we consider the GQIM system with N_{t} transmit and N_{r} receiver antennas, in which the normalized complex TSV $\bar{\mathbf{S}} \in C^{N_{\text{t}}\times 1}$ are transmitted over the MIMO Rayleigh fading channel expressed by $\mathbf{H} \in C^{N_{\text{r}}\times N_{\text{t}}}$ and the additive white Gaussian noise (AWGN) vector $\mathbf{n} \in C^{N_{\text{r}}\times 1}$. Consequently, the received signal $\mathbf{y}$ is expressed by (18), as shown at the bottom of the page, where $\rho_1 = \frac{N_{\text{t}}}{2} + \bar{\alpha}$, $\rho_2 = \frac{N_{\text{t}}}{2} + \bar{\beta}$, $\rho_3 = \frac{N_{\text{t}}}{4} + \gamma$, $\rho_4 = \frac{3N_{\text{t}}}{4} + \bar{\gamma}$, $\mathbf{H} = [\mathbf{h}_1, \cdots, \mathbf{h}_\tau, \cdots, \mathbf{h}_{N_{\text{t}}}]^T$ describe the MIMO Rayleigh fading channel coefficient matrix between the transmitter and the receiver in the proposed GQIM system, whose entries are independent and identically distributed (i.i.d.) complex-valued Gaussian random variables with zero mean and a variance of unity-power, namely $\mathcal{CN}(0, 1)$, $\mathbf{h}_\tau$ denotes the τ-th column of the channel matrix $\mathbf{H}$. $\mathbf{n}$ is the AWGN vector with zero mean and a variance of σ_{n}^2, namely $\mathcal{CN}(0, \sigma_n^2)$.

1) ML DETECTION

At the receiver of the GQIM system portrayed in Fig. 1, the joint maximum likelihood (ML) detection is employed to recover the original information bits. Then, the formula expression of ML algorithm for detecting the received signal vectors is given by

$$\left[\hat{\alpha}, \hat{\bar{\alpha}}, \hat{\beta}, \hat{\bar{\beta}}, \hat{\gamma}, \hat{\bar{\gamma}}, \hat{I}_{\text{k}}, \hat{I}_{\mathbf{V}}, \hat{S}_{3\text{D}}\right] = \arg \min_{\alpha,\bar{\alpha},\beta,\bar{\beta},\gamma,\bar{\gamma},I_{\text{k}},I_{\mathbf{V}},S_{3\text{D}}} \left\| \mathbf{y} - \frac{\mathbf{H}\cdot\mathbf{S}}{\sqrt{2\cdot E_{\text{av}}}} \right\|^2 , \tag{19}$$

where $\hat{\alpha}$, $\hat{\bar{\alpha}}$, $\hat{\beta}$, $\hat{\bar{\beta}}$, $\hat{\gamma}$, $\hat{\bar{\gamma}}$ are the detected AI vector indications, $\hat{I}_{\text{k}}$ is the detected sign indication bit, $\hat{I}_{\mathbf{V}}$ is the detected TSV indication bit, $\hat{S}_{3\text{D}}$ is the detected E3D constellation symbol.

2) LOW-COMPLEXITY ML DETECTION

Since ML detector is generally too complex to be implemented for the computational complexity of detection at the receiver, a method of lowing detection complexity for GQIM is necessary. Assuming the channel state information is known at the receiver, to reduce the detection complexity, a low-complexity ML detector is proposed for GQIM. The design rules are divided into two steps, as follows

1) Eliminating the channel matrix $\mathbf{H}$ from the received signal $\mathbf{y}$.
2) Based on the above step, implementing the ML detection algorithm.

Specifically, in the first step, utilizing the coefficient of $(\mathbf{H}^H\mathbf{H})^{-1}\mathbf{H}^H$ to eliminate the channel matrix $\mathbf{H}$, thus it has $\tilde{\mathbf{y}} = (\mathbf{H}^H\mathbf{H})^{-1}\mathbf{H}^H\cdot\mathbf{y}$, where $(\cdot)^H$ and $(\cdot)^{-1}$ denote respectively conjugate transpose and inverse of matrix. Then, implement the ML detection algorithm, which may be expressed by

$$\left[\hat{\alpha}, \hat{\bar{\alpha}}, \hat{\beta}, \hat{\bar{\beta}}, \hat{\gamma}, \hat{\bar{\gamma}}, \hat{I}_{\text{k}}, \hat{I}_{\mathbf{V}}, \hat{S}_{3\text{D}}\right] = \arg \min_{\alpha,\bar{\alpha},\beta,\bar{\beta},\gamma,\bar{\gamma},I_{\text{k}},I_{\mathbf{V}},S_{3\text{D}}} \left\| \tilde{\mathbf{y}} - \frac{\mathbf{S}}{\sqrt{2\cdot E_{\text{av}}}} \right\|^2 . \tag{20}$$

$$\begin{aligned}
\mathbf{y} &= \mathbf{H}\cdot\bar{\mathbf{S}} + \mathbf{n} \\
&= \begin{cases} \frac{1}{\sqrt{2\cdot E_{\text{av}}}}\cdot\mathbf{H}\cdot\mathbf{V} + \mathbf{n}, & \zeta = 1 \\ \frac{1}{\sqrt{2\cdot E_{\text{av}}}}\cdot\mathbf{H}\cdot\tilde{\mathbf{V}} + \mathbf{n}, & \zeta = 2 \end{cases} \\
&= \begin{cases} \frac{1}{\sqrt{2\cdot E_{\text{av}}}}\cdot\mathbf{H}\cdot\left(\begin{bmatrix}\mathbf{X}\\ \bar{\mathbf{X}}\end{bmatrix}\cdot\lambda + \begin{bmatrix}\mathbf{Y}\\ \bar{\mathbf{Y}}\end{bmatrix}\cdot\tilde{\lambda}\right) + \mathbf{n}, & \zeta = 1 \\ \frac{1}{\sqrt{2\cdot E_{\text{av}}}}\cdot\mathbf{H}\cdot\left(\begin{bmatrix}\mathbf{X}\\ \bar{\mathbf{Y}}\end{bmatrix}\cdot\lambda + \begin{bmatrix}\mathbf{Y}\\ \bar{\mathbf{X}}\end{bmatrix}\cdot\tilde{\lambda}\right) + \mathbf{n}, & \zeta = 2 \end{cases} \\
&= \begin{cases} (\mathbf{h}_\alpha + \mathbf{h}_{\rho_1})\cdot\frac{S_{3\text{D},x}}{\sqrt{2\cdot E_{\text{av}}}}\cdot\lambda + [(\mathbf{h}_\beta + \mathbf{h}_{\rho_2})\cdot\frac{S_{3\text{D},y}}{\sqrt{2\cdot E_{\text{av}}}} + (\mathbf{h}_{\rho_3} + \mathbf{h}_{\rho_4})\cdot\frac{S_{3\text{D},z}}{\sqrt{2\cdot E_{\text{av}}}}]\cdot\tilde{\lambda} + \mathbf{n}, & \zeta = 1 \\ (\mathbf{h}_\alpha\cdot\frac{S_{3\text{D},x}}{\sqrt{2\cdot E_{\text{av}}}} + \mathbf{h}_{\rho_2}\cdot\frac{S_{3\text{D},y}}{\sqrt{2\cdot E_{\text{av}}}} + \mathbf{h}_{\rho_4}\cdot\frac{S_{3\text{D},z}}{\sqrt{2\cdot E_{\text{av}}}})\cdot\lambda + (\mathbf{h}_\beta\cdot\frac{S_{3\text{D},y}}{\sqrt{2\cdot E_{\text{av}}}} + \mathbf{h}_{\rho_3}\cdot\frac{S_{3\text{D},z}}{\sqrt{2\cdot E_{\text{av}}}} + \mathbf{h}_{\rho_1}\cdot\frac{S_{3\text{D},x}}{\sqrt{2\cdot E_{\text{av}}}}) & \\ \qquad\cdot\tilde{\lambda} + \mathbf{n}, & \zeta = 2 \end{cases}
\end{aligned} \tag{18}$$

Furthermore, the computational complexity comparison of GQIM with that of other systems will be provided in TABLE 5.

V. PERFORMANCE ANALYSIS

In the section, the spectral efficiency and squared MED, the average bit error probability (BEP) for the GQIM system are provided. Moreover, the spatial index bits transmitted and computational complexity in the GQIM system are analyzed and compared with the SM, QSM, ESM, QIM-TDC and SM-SC systems.

A. SPECTRAL EFFICIENCY AND SQUARED MED

According to the above-mentioned design and analysis, the spectral efficiency (b/s/Hz) in a GQIM symbol period for the GQIM system is calculated by

$$\begin{aligned}\eta^{\mathrm{GQIM}} &= I_{\mathrm{s}} + I_{\mathrm{SI}} \\ &= I_{\mathrm{s}} + I_{\mathrm{AI}} + I_{\mathrm{k}} + I_{\mathbf{V}} \\ &= \log_2 M + 2\log_2 \frac{N_{\mathrm{t}}}{2} + 4\log_2 \frac{N_{\mathrm{t}}}{4} + I_{\mathrm{k}} + I_{\mathbf{V}} \\ &= \log_2 M + 6\log_2 N_{\mathrm{t}} - 8 \end{aligned} \tag{21}$$

Then, to show the improvement of GQIM in terms of the spectral efficiency, we make a comparison of GQIM with other schemes such as QSM, QIM-TDC and SM-SC. According to [13], [21], and [23], the spectral efficiencies for QSM, QIM-TDC and SM-SC with the modulation order M and N_{t} transmit antennas are respectively given by

- QSM: $\eta^{\mathrm{QSM}} = \log_2 M + 2\log_2 N_{\mathrm{t}}$
- QIM-TDC with 3D constellation: $\eta^{\mathrm{QIM-TDC}} = \log_2 M + \log_2 N_{\mathrm{t}} + \left\lfloor \log_2 C_{N_{\mathrm{t}}}^2 \right\rfloor$
- SM-SC with 3D constellation: $\eta^{\mathrm{SM-SC}} = \log_2 M + \left\lfloor \log_2 C_{N_{\mathrm{t}}}^3 \right\rfloor + 3.$

where $\lfloor \cdot \rfloor$ denotes the floor operation. When employing the same modulation order M and N_{t} transmit antennas, GQIM has the greater spectral efficiency. For instance, $N_{\mathrm{t}} = 8$, $\eta^{\mathrm{QSM}} = \log_2 M + 6$, $\eta^{\mathrm{QIM-TDC}} = \log_2 M + 7$, $\eta^{\mathrm{SM-SC}} = \log_2 M + 8$, and $\eta^{\mathrm{GQIM}} = \log_2 M + 10$. Obviously, it can be seen that more 4, 3, 2 information bits than QSM, QIM-TDC, SM-SC are achieved, respectively.

Furthermore, based on the design of GQIM and various systems reported in [2], [13], [19], [21]–[23], the squared MEDs $\bar{d}^2_{\mathbf{S},\min}$ for the SM, QSM, ESM, QIM-TDC, GSM-MIM, SM-SC and GQIM systems, which may be calculated by

$$\bar{d}^2_{\mathbf{S},\min} = \min_{\bar{\mathbf{S}} \neq \hat{\bar{\mathbf{S}}}} \left\| \bar{\mathbf{S}} - \hat{\bar{\mathbf{S}}} \right\|^2, \tag{22}$$

are summarized as:

- SM: $\bar{d}^2_{\mathbf{S},\min} = 4/E^{\mathrm{SM}}_{\mathrm{av}}$.
- QSM: $\bar{d}^2_{\mathbf{S},\min} = 2/E^{\mathrm{QSM}}_{\mathrm{av}}$.
- ESM: $\bar{d}^2_{\mathbf{S},\min} = 4/E^{\mathrm{ESM}}_{\mathrm{av}}$.
- QIM-TDC: $\bar{d}^2_{\mathbf{S},\min} = 2/E^{\mathrm{QIM-TDC}}_{\mathrm{av}}$.

TABLE 3. The squared MED $\bar{d}^2_{\mathbf{S},\min}$ with two cases of both $N_{\mathrm{t}} = 8$, $\eta = 13$ (b/s/Hz) and $N_{\mathrm{t}} = 16$, $\eta = 19$ (b/s/Hz).

Systems	13 (b/s/Hz)	19 (b/s/Hz)
SM [2]	4/682	4/21162
QSM [13]	2/82	2/1322
ESM [19]	4/47.875	-
QIM-TDC [21]	2/11	2/33.65625
GSM-MIM [22]	4/30	4/34
SM-SC [23]	2/8	2/16.25
GQIM	1/4	1/4

- GSM-MIM: $\bar{d}^2_{\mathbf{S},\min} = 4/E^{\mathrm{GSM-MIM}}_{\mathrm{av}}$.
- SM-SC: $\bar{d}^2_{\mathbf{S},\min} = 2/E^{\mathrm{SM-SC}}_{\mathrm{av}}$.
- GQIM: $\bar{d}^2_{\mathbf{S},\min}$ that is obtained by (16) and (17).

where E^{ψ}_{av} denote the average energy per TSV of the ψ system.

For instance, combing with the analysis of TABLE 4, $\bar{d}^2_{\mathbf{S},\min}$ for various systems at the scenarios of transmit antennas ($N_{\mathrm{t}} = 8, 16$) and spectral efficiencies 13, 19 (b/s/Hz) are summarized in TABLE 3. Note that GSM-MIM with $(n', n'', L, \tilde{L},)$ and $(TX_1, TX_2) = (\frac{N_{\mathrm{t}}}{2}, \frac{N_{\mathrm{t}}}{2})$ reported in [22], where n', n'' denote the number of the modulated L-PAM, $\tilde{L}$-QAM constellations, respectively. At the scenarios of 13, 19 b/s/Hz, GSM-MIM respectively adopt the two groups of parameters $(1, 1, 4, 32)$ and $(1, 2, 2, 16 - 32)$, where x-yQAM denotes that xQAM and yQAM are simultaneously employed. Obviously, compared with the squared MED of other systems, It can be seen from TABLE 3 that the GQIM system has the advantage in terms of the squared MED. Especially, at the scenario of 19 b/s/Hz, the squared MED $\frac{1}{4}$ of GQIM is far greater than the squared MED $\frac{4}{21162}$ of SM and $\frac{2}{1322}$ of QSM.

B. COMPARISON OF THE SPATIAL INDEX BITS

According to the relation between the spatial index bits and the modulation order of the modulated symbol, the number of spatial index bits is $I_{\mathrm{SI}} = \eta - \log_2 \Upsilon$ at the same configuration for various systems, where Υ denotes the size of modulation order in various systems. In TABLE 4, based on the analysis of (21), we compare the number of spatial index bits I_{SI} of GQIM with that of various systems. TABLE 4 shows that GQIM delivers more spatial index bits than other systems at the same configuration of both transmit data rate and N_{t} transmit antennas, especially this case that N_{t} is larger. In other words, the more spatial index bits are transmitted, the smaller the modulation order of the employed constellation becomes. It implies that the squared MED between the TSVs, which mainly determine the pairwise error probability (PEP) at high SNR, will be increased for enhancing the BER performance. For instance, at the same transmit rate of 13 (b/s/Hz) shown in TABLE 4, the number of spatial index bits transmitted are 10, 8, 7, 6, 6, 3 bits for the GQIM, SM-SC, QIM-TDC, ESM, QSM and SM systems, respectively. Consequently, the modulation order of the E3D signal constellation employed by GQIM is only 8, while the SM-SC, QIM-TDC and ESM

TABLE 4. The spatial index bits comparison between the GQIM system and the SM, QSM, ESM, QIM-TDC and SM-SC systems.

Schemes	$N_t = 8, \eta = 13$ (b/s/Hz)		$N_t = 16, \eta = 19$ (b/s/Hz)	
	Constellation	Spatial Index Bits	Constellation	Spatial Index Bits
SM [2]	1024QAM	3	32768QAM	4
QSM [13]	128QAM	6	2048QAM	8
ESM [19]	64QAM	6	–	–
QIM-TDC [21]	64-3DCII	7	512-3DCII	10
SM-SC [23]	32-3DCII	8	128-3DCII	12
GQIM	8-ary E3D	10	8-ary E3D	16

systems need to employ 32-ary 3D constellation, 64-ary 3D constellation and 64QAM, respectively. Especially, the SM system needs to employ 1024QAM constellation whose modulation order is very large. Thus, it can be seen that the GQIM system has a certain advantage in terms of the number of modulation order.

C. COMPUTATIONAL COMPLEXITY

Assuming the employment of ML detector at the receiver, we compare the computational complexity of GQIM and other schemes (e.g. QSM, QIM-TDC, SM-SC) in TABLE 5. The complexity is measured in terms of the required numbers of addition and real multiplication. From TABLE 5, it can been seen that the computational complexity of GQIM is bigger than that of other systems. However, through the proposed low-complexity ML detector, the computational complexity of GQIM is significantly reduced. In TABLE 5, D denotes the number of dimension of the signal constellation used in SM-SC. Note that, the low-complexity ML detector of Eq.(20) needs the $2^{I_\mathbf{B}} \cdot (4N_r - 1)$ number of additions and $2^{I_\mathbf{B}} \cdot 4N_r$ number of multiplications; besides that, $\tilde{\mathbf{y}} = (\mathbf{H}^H\mathbf{H})^{-1}\mathbf{H}^H \cdot \mathbf{y}$ also needs $2N_t \cdot N_r \cdot (2N_t + 1)$ number of additions and $4N_t \cdot N_r \cdot (2N_t + 1)$ number of multiplications.

D. BIT ERROR PROBABILITY

Assumming that the TSV $\mathbf{S}$ transmitted is detected as $\hat{\mathbf{S}}$. The well-known conditional PEP [24] for the GQIM system may be given by (23), as shown at the bottom of the page, where $\xi = \sum_{r=1}^{N_r} 2 \cdot \Re\{[f_r(\frac{\hat{\mathbf{S}}}{\sqrt{2 \cdot E_{\text{av}}}}) - f_r(\frac{\mathbf{S}}{\sqrt{2 \cdot E_{\text{av}}}})] \cdot n_r^*\} = \sum_{r=1}^{N_r} 2(\xi_1 + \xi_2)$, $\xi_1 = \Re[f_r(\frac{\hat{\mathbf{S}}}{\sqrt{2 \cdot E_{\text{av}}}}) - f_r(\frac{\mathbf{S}}{\sqrt{2 \cdot E_{\text{av}}}})] \cdot \Re(\mathbf{n}_r)$, $\xi_2 = \Im[f_r(\frac{\hat{\mathbf{S}}}{\sqrt{2 \cdot E_{\text{av}}}}) - f_r(\frac{\mathbf{S}}{\sqrt{2 \cdot E_{\text{av}}}})] \cdot \Im(\mathbf{n}_r)$, where ξ is the Gaussian random variable with zero mean and variance of $\sum_{r=1}^{N_r} 2\sigma_n^2 \cdot |f_r(\frac{\mathbf{S}}{\sqrt{2 \cdot E_{\text{av}}}}) - f_r(\frac{\hat{\mathbf{S}}}{\sqrt{2 \cdot E_{\text{av}}}})|^2$. Note that $f\left(\frac{\mathbf{S}}{\sqrt{2 \cdot E_{\text{av}}}}\right) = \frac{\mathbf{H} \cdot \mathbf{S}}{\sqrt{2 \cdot E_{\text{av}}}}$, $(\cdot)^*$ denotes the conjugation operation, $\Re(\phi)$ and $\Im(\phi)$ denote the real and imaginary part of the ϕ vector, respectively. $Q(\cdot)$ denotes the Gaussian Q function, $Q(x) = \frac{1}{\pi}\int_0^{\frac{\pi}{2}} \exp\left(\frac{-x^2}{2\sin^2\theta}\right) d\theta$.

According to [24], the closed-form expression of the expectation of the conventional PEP in (23) can be

$$
\begin{aligned}
P\left(\mathbf{S} \to \hat{\mathbf{S}} \middle| \mathbf{H}\right) &= P\left(\left\|\mathbf{y} - \frac{\mathbf{H} \cdot \mathbf{S}}{\sqrt{2 \cdot E_{\text{av}}}}\right\|^2 > \left\|\mathbf{y} - \frac{\mathbf{H} \cdot \hat{\mathbf{S}}}{\sqrt{2 \cdot E_{\text{av}}}}\right\|^2 \middle| \mathbf{H}\right) \\
&= P\left(\left\|\mathbf{y} - f(\frac{\mathbf{S}}{\sqrt{2 \cdot E_{\text{av}}}})\right\|^2 > \left\|\mathbf{y} - f(\frac{\hat{\mathbf{S}}}{\sqrt{2 \cdot E_{\text{av}}}})\right\|^2 \middle| \mathbf{H}\right) \\
&= P\left(\sum_{r=1}^{N_r}\left|\mathbf{y}_r - f_r(\frac{\mathbf{S}}{\sqrt{2 \cdot E_{\text{av}}}})\right|^2 > \sum_{r=1}^{N_r}\left|\mathbf{y}_r - f_r(\frac{\hat{\mathbf{S}}}{\sqrt{2 \cdot E_{\text{av}}}})\right|^2 \middle| \mathbf{H}\right) \\
&= P\left(\sum_{r=1}^{N_r}|\mathbf{n}_r|^2 > \sum_{r=1}^{N_r}\left|(f_r(\frac{\mathbf{S}}{\sqrt{2 \cdot E_{\text{av}}}}) - f_r(\frac{\hat{\mathbf{S}}}{\sqrt{2 \cdot E_{\text{av}}}})) + \mathbf{n}_r\right|^2 \middle| \mathbf{H}\right) \\
&= P\left(\xi > \sum_{r=1}^{N_r}\left|f_r(\frac{\mathbf{S}}{\sqrt{2 \cdot E_{\text{av}}}}) - f_r(\frac{\hat{\mathbf{S}}}{\sqrt{2 \cdot E_{\text{av}}}})\right|^2 \middle| \mathbf{H}\right) \\
&= Q\left(\sqrt{\frac{\sum_{r=1}^{N_r}\left|f_r(\mathbf{S}) - f_r(\hat{\mathbf{S}})\right|^2}{4 \cdot E_{\text{av}} \cdot \sigma_n^2}}\right),
\end{aligned}
\tag{23}
$$

TABLE 5. The computational complexity comparisons between the GQIM system and the SM, QSM, QIM-TDC and SM-SC systems.

Schemes	Number of additions	Number of multiplications
SM [2]	$2^{I_B} \cdot (6N_r - 1)$	$2^{I_B} \cdot 8N_r$
QSM [13]	$2^{I_B} \cdot (6N_r - 1)$	$2^{I_B} \cdot 8N_r$
QIM-TDC [21]	$2^{I_B} \cdot (8N_r - 1)$	$2^{I_B} \cdot 10N_r$
SM-SC [23]	$2^{I_B} \cdot [(2D+2)N_r - 1]$	$2^{I_B} \cdot 4N_r \cdot (\frac{D}{2} + 1)$
GQIM using ML	$2^{I_B} \cdot (14N_r - 1)$	$2^{I_B} \cdot 16N_r$
GQIM using low-complexity ML	$2^{I_B} \cdot (4N_r - 1) + 2N_t \cdot N_r \cdot (2N_t + 1)$	$2^{I_B} \cdot 4N_r + 4N_t \cdot N_r \cdot (2N_t + 1)$

obtained by

$$\bar{P}_e(\mathbf{S} \to \hat{\mathbf{S}}) = E_{\mathbf{H}}\left\{P(\mathbf{S} \to \hat{\mathbf{S}}\,|\mathbf{H})\right\} = \left(\frac{1-\mu}{2}\right)^{N_r} \cdot \sum_{k=0}^{N_r-1} C_{N_r-1+k}^{k} \cdot \left(\frac{1+\mu}{2}\right)^{k}, \quad (24)$$

where $\mu = \sqrt{\frac{\bar{\tau}}{1+\bar{\tau}}}$ with $\tau = E_{\mathbf{H}}\left\{\frac{\left|\mathbf{H}\cdot\mathbf{S} - \mathbf{H}\cdot\hat{\mathbf{S}}\right|^2}{4\cdot E_{av}\cdot\sigma_n^2}\right\}$, C_a^b is the combination of operation and denotes choosing b out of a elements.

Then, based on the union bound theory reported in [24], the upper bound on the average BEP performance of GQIM can be derived as

$$P_b \le \frac{1}{I_B \cdot 2^{I_B}} \sum_{v=1}^{2^{I_B}} \sum_{w=1}^{2^{I_B}} \bar{P}_e\left(\mathbf{S}_\omega \to \mathbf{S}_{\bar{\omega}}\right) \cdot e\left(\mathbf{S}_\omega \to \mathbf{S}_{\bar{\omega}}\right), \quad (25)$$

where $e\left(\mathbf{S}_\omega \to \mathbf{S}_{\bar{\omega}}\right)$ denotes the total number of erroneous bits occurring in the specific event when $\mathbf{S}_\omega \neq \mathbf{S}_{\bar{\omega}}$.

VI. NUMERICAL RESULTS AND DISCUSSIONS

In this section, simulation results using the Monte Carlo method are provided to verify the effectiveness and advantage of the proposed GQIM system. Assuming that the TSV symbol is transmitted over the Rayleigh fading channel with $\mathcal{CN}(0, 1)$ and the AWGN with $\mathcal{CN}(0, \sigma_n^2)$. Moreover, at the receiver, the perfect channel state information is known and the original information bits are retrieved by utilizing the ML detector. In our simulation results, according to the working principle given in Fig. 2, the 8, 16, 32-ary E3D constellations that are employed for the GQIM system, are respectively obtained by rotating the 4QAM symbols $\in \{\pm 1 \pm 1j\}$, 8-ary 2D QAM constellation symbols $\in \{\pm 1 \pm 1j, \pm 2 \pm 2j\}$ or 8PSK constellation symbols, 16-ary 2D QAM constellation symbols $\in \{\pm 1 \pm 1j, \pm 2 \pm 2j, \pm 1 \pm 3j, \pm 3 \pm 1j\}$, and considering that SM-SC with M'-ary 3D constellation (namely the parameters of $(3, M')$), GSM with two active transmit antennas ($N_a = 2$), GSM-MIM with $(n', n'', L, \tilde{L},)$ and $(TX_1, TX_2) = (\frac{N_t}{2}, \frac{N_t}{2})$ reported in [18], where n', n'' denote the number of the modulated L-PAM, $\tilde{L}$-QAM constellations, respectively. Note that x-yQAM in simulation diagram denote that xQAM and yQAM are simultaneously employed.

Fig. 3 aims at examining the effectiveness and feasibility of the proposed GQIM system. According to the Eq. (24),

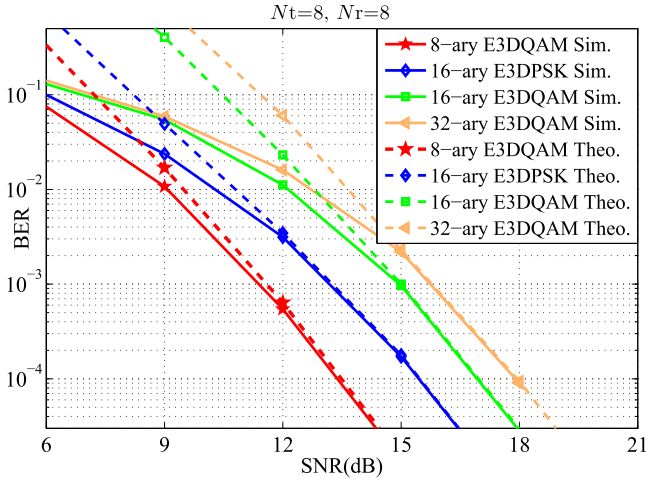

FIGURE 3. BER curves comparison of the theoretical and simulation results for the proposed GQIM system using $[N_t, N_r] = [8, 8]$ and 13 (Red line), 14 (Blue and Green lines), 15 (Orange line) b/s/Hz.

in scenarios of $[N_t, N_r] = [8, 8]$ and different transmit rates: 13, 14, 15 bits/s/Hz, the theoretical average BEP curves of the GQIM system with the 8, 16, 32-ary E3D constellations are depicted and compared with the curves of simulation results in Fig. 3. Note that in Fig. 3 M-ary E3DQAM and 16-ary E3DPSK constellations are respectively obtained by rotating N-ary 2D QAM and 8PSK constellations, and the transmit rates is obtained by Eq. (21). At the same transmit data rates, it can be observed that, since the TSV symbol is seriously disturbed and deteriorated by the fading channel response and the Gaussian white noise in lower SNR region, it has a lot of difference between the theoretical curves and the simulation curves. However, due to that the higher the SNR is, the less the interference of the Gaussian white noise on the TSV symbol is, it has a good match with both the theoretical curves (dashed lines) and the simulation curves (solid lines) in higher SNR region. Hence, it can be seen from Fig. 3 that the proposed GQIM system is feasible and effective in terms of theory and simulation results.

In Fig. 4 with $[N_t, N_r] = [8, 8]$ and 13 bits/s/Hz, the simulation result for the GQIM system with 8-ary E3DQAM constellation are depicted as the blue line with asterisk marker. Furthermore, Fig. 4 also depicts the BER curves for the GSM-MIM with the parameters of (1,1,4,32), QIM-TDC with 64-3DCII constellation that is provided in [17], GSM with both 16QAM and 32QAM, ESM with 64QAM and

QSM with 128QAM, SM-SC with the parameters of (3,32). According to the analysis of the squared MED provided by TABLE 3, at the spectral efficiency of 13 b/s/Hz, since GQIM has bigger squared MED than GSM, ESM, QSM, GSM-MIM and QIM-TDC, it will have better BER performance. Furthermore, although the squared MED of GQIM is equal to that of the SM-SC system, GQIM has also better performance due to that GQIM achieves the transmit diversity based on the above-mentioned design. From Fig. 4, it can be observed that the GQIM system achieves significantly more SNR gains than the existing classic systems such as GSM-MIM, QIM-TDC, SM-SC, GSM, ESM and QSM. At the BER of 10^{-4}, the GQIM system achieves approximately 1.7 dB over SM-SC, 2 dB over QIM-TDC, 3.4 dB over GSM-MIM, 4 dB over GSM, 4 dB over ESM, 10.5 dB over QSM in terms of SNR gain.

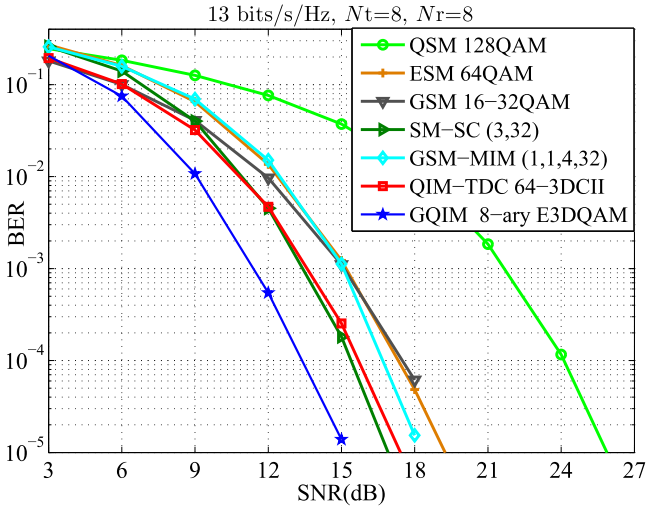

FIGURE 4. BER performance comparison of GQIM with the QSM, ESM, GSM, QIM-TDC, GSM-MIM and SM-SC systems using $[N_t, N_r] = [8, 8]$ and 13 b/s/Hz.

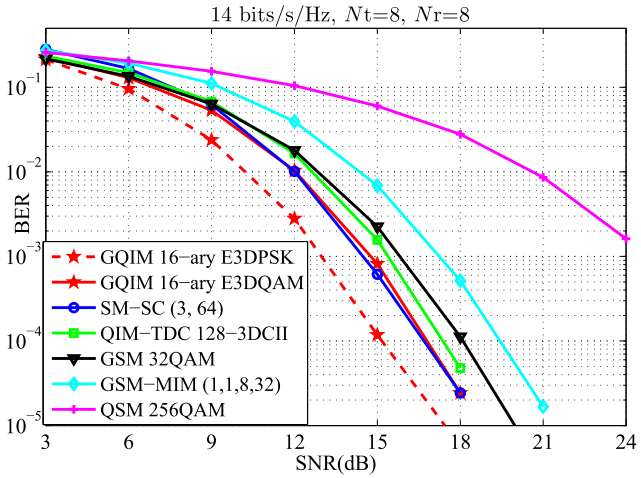

FIGURE 5. BER performance comparison of GQIM with the QSM, GSM, QIM-TDC, SM-SC, GSM-MIM systems using $[N_t, N_r] = [8, 8]$ and 14 b/s/Hz.

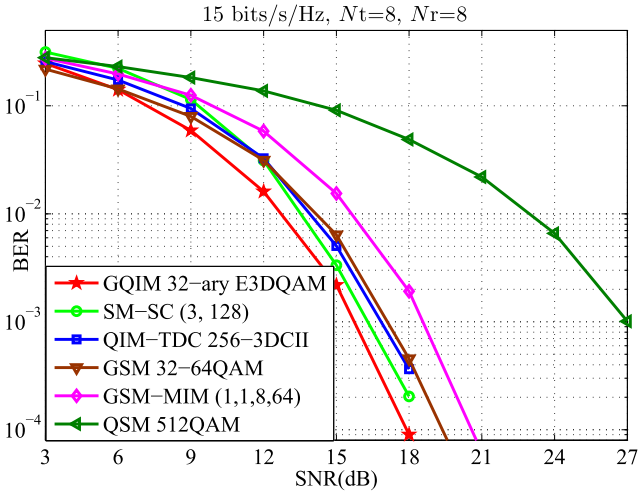

FIGURE 6. BER performance comparison of GQIM and with the QSM, GSM, QIM-TDC, GSM-MIM, SM-SC systems using $[N_t, N_r] = [8, 8]$ and 15 b/s/Hz.

In order to further prove that the GQIM system using other E3DQAM constellations also has better BER performance than the existing classic systems, Fig. 5 depicts the BER versus SNR curves at 14 bits/s/Hz and $[N_t, N_r] = [8, 8]$ for the GQIM system with both 16-ary E3DQAM and 16-ary E3DPSK that are respectively obtained by rotating 8-ary 2D QAM constellation (i.e., $\in \{\pm 1 \pm 1j, \pm 2 \pm 2j\}$) and 8PSK constellation, the SM-SC system with (3, 64), the QIM-TDC system with 128-3DCII constellation that is provided in [17], the GSM system with 32QAM, the GSM-MIM system with (1,1,8,32), the QSM system with 256QAM. Similarly to the analysis of Fig. 4, due to the advantage of both the bigger squared MED and the achievable transmit diversity gain for the GQIM system, it can be seen from Fig. 5 that the GQIM system with 16-ary E3DPSK has greatly better BER performance than other systems. In addition, although the squared MED ($\frac{1}{10}$) of GQIM system with 16-ary E3DQAM is smaller than that ($\frac{2}{11}$) of SM-SC, the performance curve of GQIM is close to that of SM-SC due to the achievable transmit diversity gain.

In Fig. 6, the BER versus SNR curves of 15 b/s/Hz with $[N_t, N_r] = [8, 8]$ are plotted for the GQIM, QSM, GSM, QIM-TDC, GSM-MIM, SM-SC systems. According to the analysis of TABLE 4, In this case that only one signal constellation is employed, the number of spatial index bits achieved for the GQIM, QSM, QIM-TDC, SM-SC systems are respectively 10, 6, 7, 8 information bits. Hence, 32-ary E3DQAM, 512QAM, 256-3DCII and 128-3DCII are needed to be employed for the GQIM, QSM, QIM-TDC, SM-SC systems, respectively. Obviously, at the same transmit rate, the GQIM system using the lower-order signal constellation will have the certain advantage in terms of the squared MED. Then, through the calculation, the squared MED for the GQIM, QSM, QIM-TDC, SM-SC systems are respectively $\frac{1}{15}$, $\frac{2}{330}$, $\frac{2}{23.1875}$, $\frac{2}{16.25}$. Since the GQIM system has the bigger MED than QSM, except for the SM-SC and QIM-TDC

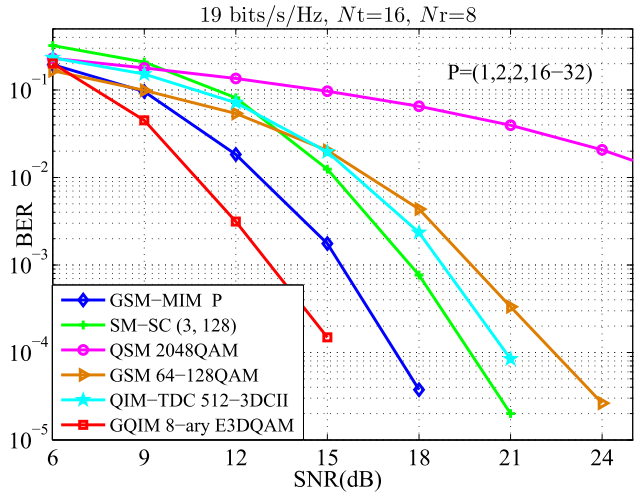

FIGURE 7. BER performance comparison of GQIM and of the QSM, GSM, GSM-MIM, QIM-TDC, SM-SC systems using $[N_t, N_r] = [16, 8]$ and 19 b/s/Hz.

systems, the GQIM system has better BER performance than the QSM system. In addition, although the squared MED of GQIM is inferior to that of the SM-SC and QIM-TDC systems, since the GQIM system achieves the transmit diversity, it can be observed from Fig. 6 that the GQIM system also has better BER performance than the SM-SC and QIM-TDC systems. For instance, Fig. 6 shows that, at the SNR of 10^{-3}, the SNR gains achieved by the GQIM system are about 0.6 dB over SM-SC, 1.2 dB over QIM-TDC, 11 dB over QSM. Also, 1.5 dB over GSM with 32-64QAM, 3 dB over GSM-MIM with (1, 1, 8, 64) are achieved for the GQIM system, respectively.

To verify the outstanding of the GQIM system at small-scale transmit antennas, we also make the simulation results when $N_t = 16$. In the scenario of $[N_t, N_r] = [16, 8]$ and 19 b/s/Hz, the advantage of the GQIM system is greatly significant in terms of the spatial index bits and the BER performance. According to the numerical analysis of TABLE 4, 16 information bits from the number of the transmit data rate (19 b/s/Hz) are used for the transmission of the spatial index bits in GQIM system. Consequently, only the remaining three information bits are used for the mapping of signal constellation symbol. In comparison with the SM-SC, QIM-TDC and QSM systems, more 4, 6, 8 information bits in terms of the spatial index bits are achieved for the GQIM system, respectively. Thus, for the transmission of 19 b/s/Hz, the QIM-TDC and SM-SC systems respectively employ the 512, 128-ary 3D constellation, and especially the QSM system needs to employ 2048QAM constellation, while the GQIM system only employs a 8-ary E3DQAM constellation. According to the calculation of the squared MED between the TSVs, it has $\frac{1}{4}$, $\frac{2}{16.25}$, $\frac{2}{33.65625}$, $\frac{2}{1322}$ for the GQIM, SM-SC, QIM-TDC, QSM systems, respectively. Obviously, due to the advantage of the modulation order, the GQIM system using 8-ary E3DQAM will have excellent BER performance as compared with the SM-SC, QIM-TDC, QSM systems. Observed from our simulation results in Fig. 7 that the BER versus SNR curves verify this conclusion. For instance, the GQIM system outperforms approximately 4.5 dB SNR gains over SM-SC, 5 dB over QIM-TDC, 16.5 dB over QSM at BER of 10^{-2}. Furthermore, we also compare the BER performance of the GQIM system with that of the GSM system with 64-128QAM and that of the GSM-MIM system with (1, 2, 2, 16-32). It can be seen that the excellent SNR gains for the GQIM system are also achieved. For instance, it can be observed from Fig. 7 that the SNR gains at BER value of 10^{-3} for the GQIM system are 5 dB over GSM and 2 dB over GSM-MIM.

Finally, the above-mentioned simulation results demonstrate the effectiveness and correctness of our proposed GQIM.

VII. CONCLUSION

In this paper, in order to enhance the spectral efficiency and reliability of the MIMO-based communications system, a new design scheme of GQIM system is proposed to further extend the spatial index domain such as the key and vector indications. An E3D constellation is constructed and obtained by extending the dimension of conventional 2D signal constellation. Then, through the AI modulator and vector combiner, two versions of the resulted E3D constellation are transformed into four spatial vectors. Furthermore, with the aid of the key and vector indications, a complex TSV symbol is obtained through the combination of four spatial vectors. Finally, the BEP performance and the spatial index bits are analyzed and verified the advantage of the GQIM system. Simulation results are discussed and demonstrate that the GQIM system improves the BER performance as compared with other conventional spatial modulation systems (e.g., QSM, ESM, GSM, QIM-TDC, GSM-MIM, SM-SC).

REFERENCES

[1] P. W. Wolniansky, G. J. Foschini, G. D. Golden, and R. A. Valenzuela, "V-BLAST: An architecture for realizing very high data rates over the rich-scattering wireless channel," in *Proc. URSI Int. Symp. Signals, Syst., Electron.*, Pisa, Italy, Oct. 1998, pp. 295–300.

[2] R. Y. Mesleh, H. Haas, S. Sinanovic, C. W. Ahn, and S. Yun, "Spatial modulation," *IEEE Trans. Veh. Technol.*, vol. 57, no. 4, pp. 2228–2241, Jul. 2008.

[3] J. Jeganathan, A. Ghrayeb, and L. Szczecinski, "Spatial modulation: Optimal detection and performance analysis," *IEEE Commun. Lett.*, vol. 12, no. 8, pp. 545–547, Aug. 2008.

[4] M. Renzo, H. Haas, and P. Grant, "Spatial modulation for multiple-antenna wireless systems: A survey," *IEEE Commun. Mag.*, vol. 49, no. 12, pp. 182–191, Dec. 2011.

[5] J. Jeganathan, A. Ghrayeb, L. Szczecinski, and A. Ceron, "Space shift keying modulation for MIMO channels," *IEEE Trans. Wireless Commun.*, vol. 8, no. 7, pp. 3692–3703, Jul. 2009.

[6] M. Di Renzo and H. Haas, "A general framework for performance analysis of space shift keying (SSK) modulation for MISO correlated Nakagami-*m* fading channels," *IEEE Trans. Commun.*, vol. 59, no. 1, pp. 2590–2603, Sep. 2011.

[7] S. Fang, L. Li, S. Hu, J. Tang, Z. Yue, G. Feng, and A. Pandharipande, "Layered space shift keying modulation over MIMO channels," *IEEE Trans. Veh. Technol.*, vol. 66, no. 1, pp. 159–174, Jan. 2017.

[8] J. Jeganathan, A. Ghrayeb, and L. Szczecinski, "Generalized space shift keying modulation for MIMO channels," in *Proc. IEEE 19th Int. Symp. Pers., Indoor Mobile Radio Commun.*, Sep. 2008, pp. 1–5.

[9] A. Younis, N. Serafimovski, R. Mesleh, and H. Haas, "Generalised spatial modulation," in *Proc. Asilomar Conf. Signals, Syst., Comput.*, Pacific Grove, CA, USA, Nov. 2010, pp. 1498–1502.

[10] J. Fu, C. Hou, W. Xiang, L. Yan, and Y. Hou, "Generalised spatial modulation with multiple active transmit antennas," in *Proc. IEEE Globecom Workshops*, Miami, FL, USA, Dec. 2010, pp. 839–844.

[11] J. Wang, S. Jia, and J. Song, "Generalised spatial modulation system with multiple active transmit antennas and low complexity detection scheme," *IEEE Trans. Wireless Commun.*, vol. 11, no. 4, pp. 1605–1615, Apr. 2012.

[12] T. Data, H. S. Eshqaraiah, and A. Chockalingam, "Generalized space and frequency index modulation," *IEEE Trans. Veh. Technol.*, vol. 65, no. 6, pp. 4911–4924, Jul. 2016.

[13] R. Mesleh, S. S. Ikki, and H. M. Aggoune, "Quadrature spatial modulation," *IEEE Trans. Veh. Technol.*, vol. 64, no. 6, pp. 2738–2742, Jun. 2015.

[14] D. Feng, Q. He, B. Bai, J. Zheng, and M. Liu, "Spatial modulation with multi-dimensional constellations," *IEEE Wireless Commun. Lett.*, vol. 9, no. 1, pp. 99–102, Jan. 2020.

[15] J. Freudenberger, D. Rohweder, and S. Shavgulidze, "Generalized multistream spatial modulation with signal constellations based on Hurwitz integers and low-complexity detection," *IEEE Wireless Commun. Lett.*, vol. 7, no. 3, pp. 412–415, Jun. 2018.

[16] J. Freudenberger and S. Shavgulidze, "Signal constellations based on Eisenstein integers for generalized spatial modulation," *IEEE Commun. Lett.*, vol. 21, no. 3, pp. 556–559, Mar. 2017.

[17] L. Singla and L. P. Natarajan, "Improving generalized spatial modulation using translation patterns," *IEEE Commun. Lett.*, vol. 24, no. 12, pp. 2814–2818, Dec. 2020.

[18] Z. Yigit and E. Basar, "Double spatial modulation: A high-rate index modulation scheme for MIMO systems," in *Proc. Int. Sym. Wireless Commun. Syst. (ISWCS)*, Poznan, Poland, Sep. 2016, pp. 347–351.

[19] C.-C. Cheng, H. Sari, S. Sezginer, and Y. T. Su, "Enhanced spatial modulation," *IEEE Trans. Commun.*, vol. 63, no. 6, pp. 2237–2248, Jun. 2015.

[20] C.-C. Cheng, H. Sari, S. Sezginer, and Y. T. Su, "New signal designs for enhanced spatial modulation," *IEEE Trans. Wireless Commun.*, vol. 15, no. 11, pp. 7766–7777, Nov. 2016.

[21] F. Huang, X. Liu, Z. Zhou, J. Luo, and J. Wang, "Quadrature index modulation with three-dimension constellation," *IEEE Access*, vol. 7, pp. 182335–182347, 2019.

[22] Y. Zhan and F. Huang, "Generalized spatial modulation with multi-index modulation," *IEEE Commun. Lett.*, vol. 24, no. 3, pp. 585–588, Mar. 2020.

[23] F. Huang and Y. Zhan, "Design of spatial constellation for spatial modulation," *IEEE Wireless Commun. Lett.*, vol. 9, no. 7, pp. 1097–1100, Jul. 2020.

[24] M. K. Simon and M. Alouini, *Digital Communication Over Fading Channels* (Wiley Series in Telecommunications and Signal Processing), 2nd ed. Hoboken, NJ, USA: Wiley, 2005.

ZHENYU TANG received the B.S. degree in packaging engineering and the M.E. degree in mechanical manufacture and automation from the Guangdong University of Technology, China, in 1997 and 2004, respectively. He is currently working with the School of Mechanical Engineering, Guangzhou Maritime University. His research interests include the signal processing, intelligent equipment design, and automation.

FUCHUN HUANG received the B.E. degree in electronics information engineering from Henan Polytechnic University, China, in 2008, and the M.E. degree in telecommunication and information system from Jiangsu University, China, in 2012. He is currently with the Guangzhou College of Commerce, Guangzhou, China. His current research interests include index modulation, spatial constellation design, antenna selection algorithms, and OFDM.

ZHILI ZHOU received the B.S. degree in automation engineering and the M.S. degree in communications and information system from the Zhejiang University of Technology, China, in 2001 and 2009, respectively, and the Ph.D. degree in communication engineering from Sun Yat-sen University, China, in 2018. He is currently working with the College of Electrical and Electronic Engineering, Wenzhou University. His research interests include the signal processing and artificial intelligence.

ZHIJUN LIU received the M.E. degree in mechanical manufacture and automation from the Guangdong University of Technology, China, in 2004, and the Ph.D. degree from the South China University of Technology, China, in 2013. He is with the School of Shipping and Marine Engineering, Guangzhou Maritime University, Guangzhou, Guangdong, China. His research interest includes intelligent system operation and control.

QILIN BI received the B.E. and M.E. degrees in mechanical manufacture and automation from the Guangxi University of Science and Technology, China, in 2007 and 2010, respectively, and the Ph.D. degree in mechanical manufacture and automation from the South China University of Technology, China, in 2014. He is currently working with the School of Mechanical Engineering, Guangzhou Maritime University. His research interests include the signal processing, intelligent detection, and sensing technology.